Princetonlaan 6
P.O. Box 80015
3508 TA Utrecht
The Netherlands

www.tno.nl

T +31 88 866 42 56
F +31 88 866 44 75
info-BenO@tno.nl

TNO report

TNO-034-UT-2010-0223

Reconstruction of burial history, temperature, source rock maturity and hydrocarbon generation for the NCP-2D area, Dutch Offshore

Date	December 2012
Author(s)	R. Abdul Fattah J.M. Verweij N. Witmans
Number of pages	72
Projectname	4DMod
Projectnumber	034.22774/01

Contents

1 Introduction

1.1 Mapping of the deep subsurface of the Netherlands offshore (NCP-2 project)

The detailed mapping of seven offshore areas on the Netherlands Continental Shelf was initiated in late 2005 and will be finalised in 2010. It builds on and goes one step beyond the previous regional mapping of the Netherlands onshore and offshore. In 2004 the publication of the Geological Atlas of the Subsurface of the Netherlands – onshore rounded off the onshore regional mapping project and a 'quick and dirty' offshore mapping (NCP-1 project) was completed in 2006 (viz. on the http://www.nlog.nl; Duin et al. 2006).

The main aim of the detailed mapping of seven sub-areas is to present a more comprehensive model of the subsurface to future and current operators in the oil industry and to governmental and non-governmental organisations for, amongst other things, the spatial planning of the Dutch subsurface. The deliverables include:

- 3D geological framework (depth and thickness grids)
- Rock and fluid parameters (petrophysical parameters, P, T, Vr) 3D burial histories
- Petroleum system analysis

All deliverables, such as maps, grids and graphs, can be downloaded at the http://www.nlog.nl site. When applicable, regular updates will be made available on the site.

1.1.1 Definition of mapping areas in the Netherlands offshore

Based on consultation with the exploration departments of the oil companies operating in the Netherlands it was decided to divide the offshore area into seven sub-areas (Figure 1). These areas more or less represent structural entities at the Late Jurassic to Early Cretaceous times (Figure 2). One of these sub-areas is the 2D area. Area 2D includes the Cleaver Bank Platform and parts of the Silverpit Platform, Elbow spit Platform, Step Graben and the western margin of the Dutch Central Graben.

1.1.2 Detailed mapping of the Platform areas

The detailed mapping was focussed on the assessment of the present-day stratigraphic and structural framework of the sedimentary fill of the area as well as on the properties of rocks and fluids it contains, such as reservoir porosities, pressures, salinities, source rock maturity, characteristics of oil and gas.

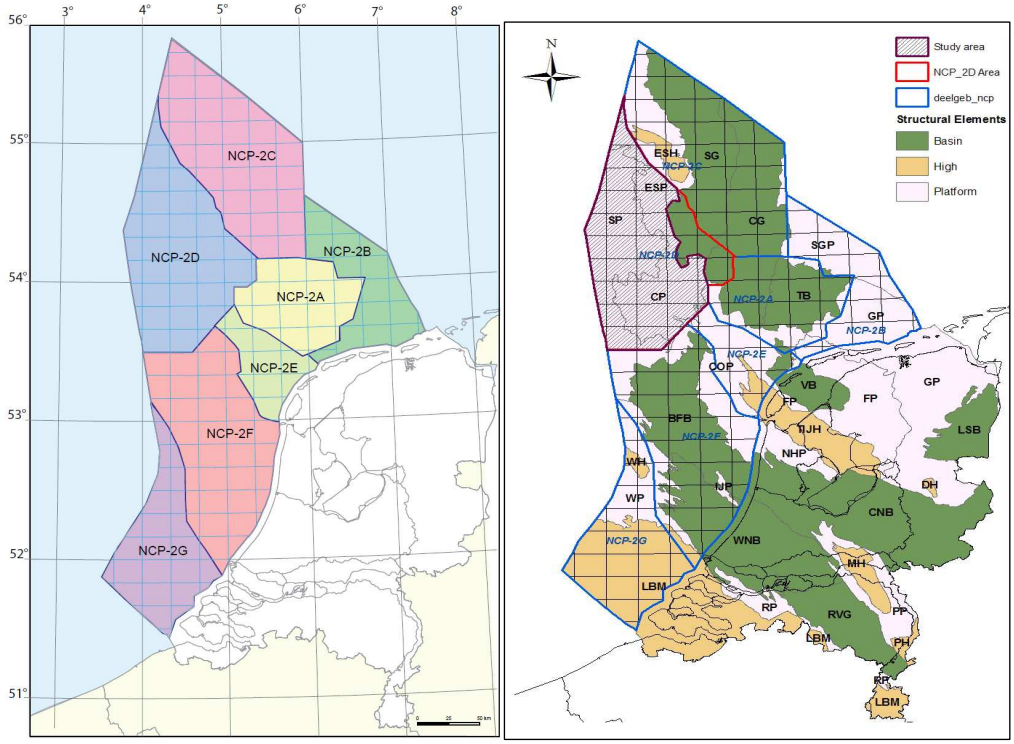

Figure 1:Major structural elements in the Netherlands with the location of study area within the NCP-2D area in the Dutch offshore. The structural settings in the region in the Late Jurassic-Early Cretaceous (Right).

1.2 Basin modelling in the Platform in the NCP-2D area

The NCP-2D area is dominated by platforms. The eastern most part of the area borders the western margins of the Central Graben and the Step Graben. The focus of this study is on the platforms that dominate the NCP-2D area; the focus is not the grabens. These platforms include the Cleaver Bank Platform (CB), Silverpit Platform (SP) and the Elbow Spit Platform (ESP).

This report presents results of 3D basin modelling of the burial history and the history of temperature, source rock maturity and timing of hydrocarbon generation in the offshore Netherlands from 320 Ma to present-day.

The platforms in the area form an important gas producing area in the Dutch offshore. The gas fields are producing from Westphalian and Upper Rotliegend sandstones and are charged from Westphalian coal seams and probably also from pre-Westphalian source rocks (De Jager & Geluk, 2007; Gerling et al. 1999). There is an increasing interest in this area and especially in the source rock properties of the Westphalian and pre-Westphalian units.
Based on geochemical analysis of gas samples, Gerling et al. (1999) suggest a mixed source for the gases in the study area. The majority of the gas originates from a sapropelic marine source rock which might be the Namurian or Dinantian shales. Terrestrial source rocks (the Westphalian Coal Measures) have also contributed with a lower degree to the gas accumulations in the area.

Interest in the Namurian source rock and reservoir characteristics is increasing because of the – hitherto largely unknown - Namurian shale gas prospectivity in addition to its role in explaining the occurrence of locally high nitrogen content in gas fields in the area. The nitrogen content of the natural gas accumulations of the study area varies from < 10 Mol% to very high values in the gas accumulations in the Carboniferous reservoirs (> 80 Mol % in D block). The possible origin of the nitrogen in the gas accumulations in North Western Europe has been subject of extensive studies for more than 10 years (Gerling et al., 1997; Krooss et al., 1995, 2005, 2006; Littke et al., 1995; Mingram et al., 2003, 2005 & Verweij, H., 2008). However, the sources of the nitrogen and the migration and accumulation processes are still not very well understood. The Namurian is thought to have contributed to a greater or lesser extent to the nitrogen charge of natural gas accumulations in the Netherlands (De Jager and Geluk, 2007). In general, variations in nitrogen content might be related to variations in origin/source rock types, as well as quality and maturity of source rocks (e.g. Kombrink et al., 2009).

The origin of the gas accumulations and the variable nitrogen content in the study area require more investigation into the temperature and maturity evolution as well as the properties of the source rock units and their spatial variation.

We use basin modelling to reconstruct key elements and processes important for evaluating the gas systems. This includes burial history (sedimentation and erosion history), basal heat flow history as well as history of temperature and source rock maturity. The focus is on the Westphalian and pre-Westphalian (Namurian and Dinantian) source rocks.

The results of the TNO mapping program provide a new 3D stratigraphic model and petrophysical properties which can be used in our model. New boundary conditions are applied which include new basal heat flow models and an updated and refined paleo surface water temperatures and paleo water depths. Model calibration data, such as temperature and vitrinite reflectance, are used from an updated in-house database.

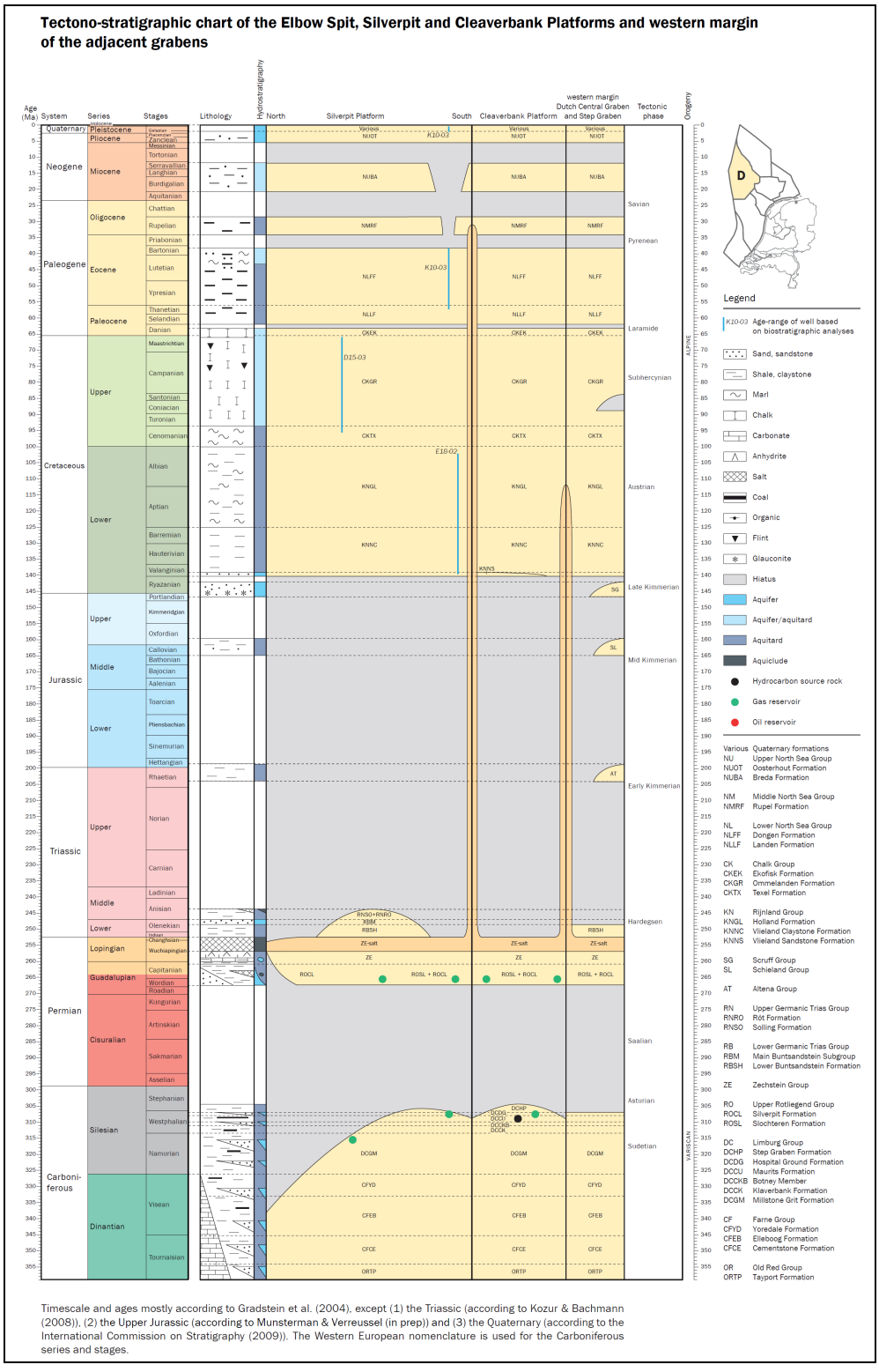

Figure 2: Tectonostratigraphic chart of the Cleaver Bank High.

1.2.1 Geological setting of the study area

Quirk (1993), De Mulder et al. (2003), TNO-NITG (2004), Duin et al. (2006) and Wong et al. (2007) and references therein provide a detailed and extensive overview of the regional geology and petroleum geology of the Netherlands and the Cleaver Bank Platform

The Cleaver Bank and the Silverpit platforms are located in the northern part of the Dutch continental shelf of the North Sea and extend over the D, E, K, and western L-quadrants. The eastern margins of the platforms are defined by a complex set of NW-SE and N-S normal faults underlying the Zechstein salt. Important phases of the geodynamic history of the area include the Carboniferous and Saalian phase of uplift and erosion, Late Permian-Triassic rifting phases, Mid and Late Kimmerian phases of erosion and rifting, and the Subhercynian and Laramide tectonic phases.

During the Early Carboniferous, the whole of the Netherlands, including the study area, was located in the foreland basin of the Variscan orogen (De Jager, 2007). The NCP-2D area was affected by late-Variscan post-orogenic tectonism in the Late Carboniferous. This resulted in wrench faulting associated with intrusive and extrusive magmatism (Ziegler, 1990). Indications for magmatic activity (intrusive) related to this phase have been reported by Van Bergen & Sissingh (2007).The collapse of the Variscan orogeny, at the Carboniferous-Permian transition, caused regional thermal uplift and erosion of a substantial part of the upper Carboniferous deposits (Saalian erosion phase).

The uplift event was followed by thermal relaxation and regional subsidence in the area. The subsidence provided accommodation for sediments which started to be deposited in the large E-W trending Southern Permian Basin (Doornenbal and Stevenson, 2010; Van Wees et al., 2000). A thick package of eolian and fluvial sediments (Slochteren Formation) and desert lake deposits (Silverpit Formation) of the Upper Rotliegend Group was deposited in the Mid Permian. This was followed by the deposition of Late Permian evaporates, carbonates and clays of the Zechstein Group in the study area.

The thermal subsidence was locally associated in the study area with minor extensional tectonics during the Early Triassic. Extensional tectonics prevailed in the Late Triassic and the Early Jurassic.

For long times, the platform areas were a deposition centre, similar to the Mesozoic extensional basins. In the Mid Jurassic, the thermal Central North Sea Dome developed and led to the uplift of much of the Dutch offshore area (Ziegler, 1990a; De Jager, 2007). The uplift is attributed to a doming event related to the prevalent extension in combination with a global fall in sea level. During Mid-Late Jurassic the regional uplift caused widespread erosion in the platform area in the NCP-2D (Mid and Late Kimmerian). The uplift varied in magnitude and impact over the study area. The erosion removed all evidence of Lower Jurassic and Upper Triassic strata over the study area (Quirk, 1993) in some places.

In Early Cretaceous times, the eustatic sea level rose. The area was gradually inundated and deposition of siliciclastic sediments took place. Regional thermal subsidence associated with sea level rise prevailed during Late Cretaceous. This lead to the deposition of the thick Chalk Group in the area. The present thickness of Chalk

succession varies over the area increasing southwards The relatively thick Cretaceous formations lay unconformably on the Zechstein formations.

Tertiary and Quaternary sediments unconformable overlie the Chalk. Another unconformity is observed in the middle of the Cenozoic section corresponding to the base of the Miocene.

1.2.2 Petroleum systems in the NCP-2D area

Figure 3 shows the distribution of the gas fields in the area. Analysis of gas samples shows that the produced gas is a mixture of wet and dry gas. The majority of the gas is generated from marine organic material (could be the Namurian or Dinantian shales). Westphalian Coal Measures is the source rock of a less percentage of the gases in the reservoirs in the area (Gerling et al., 1999). Furthermore, gas samples from the study area show relatively high content of nitrogen.
The gas is reservoired in the sandstone units of the Upper Rotliegend Group and the Limburg Group. Carboniferous reservoirs are mainly in the Westphalian A and B (Botney Mbr) and Westphalian C and D (Hospital Ground Fm) (Figure. 2).

The fields are concentrated in the Northern K and Southern D and E quadrants at depth around 3,500 to 4,000 m. Westphalian sandstones in the Cleaver Bank Platform were deposited by fluvial systems from northern sources and their reservoir quality deteriorates toward the south (De Jager and Geluk, 2007). Rotliegend reservoirs (from the Slochteren Formation) are located in D and K quadrants in the southern sector of the Cleaver Bank Platform. To the north, the Slochteren sandstones shale out into the Silverpit Formation. In the northern K blocks and adjacent areas, the shaly Silverpit Formation provides a seal for the underlying basal Slochteren sandstone (De Jager and Geluk, 2007).

The main seal in the area is the Zechstein evaporite units that cover large parts of the area. Clays and evaporites of the Silverpit Formation, inter-Westphalian shales and faults provide sealing as well (De Jager and Geluk, 2007).

The main source rocks in the area are the Coal Measures of the Carboniferous Limburg Group. In addition to the Westphalian Coal Measures, pre-Westphalian marine deposits (Namurian and Dinantian) are thought to have contributed to the gas accumulations.

Gerling et al. (1999) provides an overview of the Paleozoic source rocks in the area which includes the Dinantian, Namurian and Westphalian sediments. The Dinantian source rock in the study area comprises deltaic, coal bearing sediments of the Farne Group. The total organic carbon (TOC) in the sediments is between 0.9 – 1.9 % and the organic matter is of type III kerogen (Gerling et al., 1999).
The Namurian source rocks in the area have similar depositional settings as the Dinantian. It consists of marine and deltaic sediments known as the Millstone Grit and Epen formations. Most of the study area is underlain by Namurian marine shales. Namurian shales may include good source rocks of type II kerogen (Gerling et al., 1999).

The coal bearing source rocks of the Westphalian Maurits and Klaverbank formations are of kerogen type III. The Klaverbank Formation in the study area is age equivalent to

the Ruurlo and Baarlo formations in the southern and eastern offshore and onshore Netherlands (Van Adrichem Boogaert & Kouwe, 1993-1997).

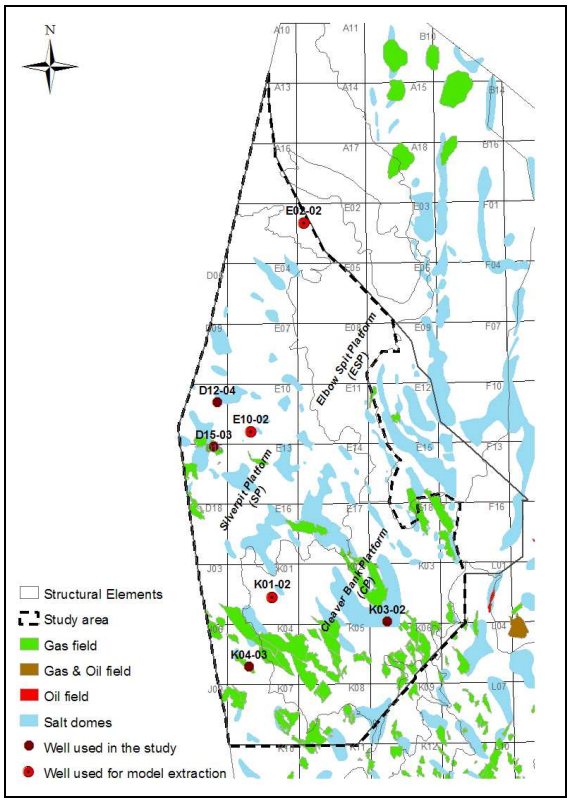

Figure 3: Map of the study area showing the distribution of major gas fields and the major structural units. The wells used in the study are indicated. Wells used for 1D extractions used for burial history, temperature and maturity analysis are given the red colour.

1.3 Basin modelling of the NCP-2D area

TNO uses 1D, 2D and 3D basin modelling (Petromod, version 11, of IES-Schlumberger) to integrate the wealth of data and information gathered and mapped in its detailed mapping programme of subareas of offshore Netherlands and to evaluate the interdependencies of the different processes that affect rocks and fluids during its geological history. Special attention is paid to processes and conditions affecting hydrocarbon potential. Here we present selected results from a full 3D reconstruction of the burial history, and the history of temperature, source rock maturity and timing of hydrocarbon generation for the Carboniferous source rocks in the Platforms from 320 Ma to present-day.

2 Basin modelling: workflow, input data and boundary conditions

Basin modelling helps to understand the evolution of the basin through time. Based on the input and the initial model (see below), the formation and the evolution of a basin are simulated. Basin modelling is also used to model various properties of the layers within the basin, such as porosity, temperature, pressure thermal maturity.. etc. For petroleum system analysis, basin modelling helps to understand the evolution of the petroleum systems through time. It is therefore used to evaluate the prospectivity of the basin. The history of maturity and hydrocarbon generation is based on the evolution of the thermal regime within the basin. This is related to the burial depth of the source rocks and the thermal gradient within the basin. Basin modelling can also help in predicting the migration paths and hydrocarbon accumulations. For more information on basin modelling the reader is referred to Hantschel & Kauerauf (2009), Allen & Allen (2005) . A simple workflow describing the main steps in basin modelling is presented below:

1- A litho-stratigraphic model of the basin is introduced. This includes thickness layers and lithological properties of the main formations in the model. This can also include the faults and their properties.
2- Properties of the main source rock units can be introduced if the purpose is to evaluate the hydrocarbon generation. This includes, the Total Organic Carbon (TOC) content and the Hydrogen index, kerogen type..etc. The kinetics that describe the generation and transformation of the organic matter is also defined.
3- Three main boundary conditions are introduced. These are: a) basal heat flow b) paleo water depth (PWD) c) the paleo surface water interface temperature (SWIT). These are used to reconstruct the evolution of the thermal gradient within the basin at various stages. It also helps in calculating the burial history of the various layers within the basin. The basal heat flow can be modelled based on tectonic concepts and the evolution of the basin.
4- It is necessary to calibrate the outcome of the model to measured data, such as temperature, vitrinite reflectance, porosity, pressure..etc. For this reason, introducing calibration data to the model and quality controlling them is an essential part of the work flow.
5- The results of the simulation are then compared to measured data (calibration process). Depending on that, model parameters are modified and the simulation is done again.

2.1 Assumptions and conditions underlying the basin modelling approach

Basin modelling deals with the computation of the time evolution from an initial geological model. The modelling requires an initial state and general assumptions and boundary conditions to be observed. We now list general assumptions and boundary conditions inherent in basin modelling:

- Geological history:
  - the model is laterally constrained: no horizontal compression or extension of the basin fill is taken into account.
  - vertical movement only (no lateral deformation of the sediments in the model, except for salt movement, if considered in the model)
  - salt movement has no direct relation to changes in stress
  - compaction of the basin fill is vertical
  - compaction is mechanical according to a vertical effective stress-based rock property model
- History pore water fluids:
  - density of pore water is constant
- Thermal history:
  - conductive heat flow

The basin modelling scenarios presented here are based on a geological model without faults and assumed open fluid flow boundaries. In addition to these general limiting assumptions and conditions, default set-ups of the modelling package influence simulation results. Such default set-ups include default relations between standard lithologies and properties through compaction approaches, porosity-permeability relations, thermal models, kinetic models; mixing rules lithology. The selection of the proper set-up is an important part of the basin modelling workflow.

2.2 Database

The basic data requirements for the 3D modelling involve: present-day geometry (stratigraphy; property/facies boundaries within stratigraphic units, fault geometries, water depth); lithological properties (lithological composition of each stratigraphic unit and eroded (part of) unit and of each facies); quantified uninterrupted time-sequence of events during geological history (3D history of sedimentation, uplift and erosion; estimated thickness of erosion; 3D history of water depth, basal heat flow, surface temperature; timing of salt movement and fault activity); calibration data (such as present-day temperatures, porosities, permeabilities, pressures, vitrinite reflectance measurements).
The results of the recent detailed mapping of the NCP-2D area provided the present-day stratigraphic and structural framework of the sedimentary fill. Calibration data (temperatures, porosities, permeabilities, pressures, vitrinite reflectance values) required for the numerical modelling, are available from an in-house database.

2.3 Basin modelling workflow

The general workflow with respect to the full 3D basin modelling of the study area included the following steps:

1- Building 3D geological model. This includes reviewing and editing the input depth maps for the different formations as well as establishing initial scenarios for erosion phases;
2- Selection proper Petromod default porosity-depth and porosity-permeability relations;
3- Running 3D model for reconstructing burial history;

4- Selection proper thermal conductivity model (using measured temperature data and published information on thermal conductivities); the default Sekiguchi model of Petromod was selected;
5- Generating heat flow boundary conditions based on the tectonic evolution of the area and using the probabilistic modelling tool PetroProb;
6- Running 3D model for reconstructing the history of hydrocarbon generation, using the Pepper and Corvi (1989)_Type III-IV F kinetic model for the Carboniferous source rocks and, and final set of source rock parameters), in this scenario no salt movement was introduced;
7- Evaluation simulation results for various scenarios.

2.4 Input: Present-day geometry

The initial 3D stratigraphic model consists of 9 stratigraphic groups. These include the Upper North Sea, Lower & Middle North Sea, Chalk, Rijnland, Schieland and Scruff, Altena, Upper Germanic Trias, Lower Germanic Trias and Zechstein groups. New maps are created and included in the model to achieve a more detailed, comprehensive and realistic model.
A Rotliegend thickness map is created and added to the model by interpolating between present-day thicknesses from wells over the whole NCP-2D area (Figure 4). The model is extended below the Rotliegend Group by adding Carboniferous layers. The Carboniferous section comprises five layers, the Step Graben, the Hospital Ground, the Maurits, the Klaverbank and the Pre-Westphalian. A basement, of 2000 m thickness, is added to the bottom of the section. The model is refined with additional maps for the Upper North Sea Group which is subdivided into 3 new layers; Quaternary, Pliocene and Miocene. The final refined and extended 3D model includes 17 layers plus the basement (Figure 5, Table 1).

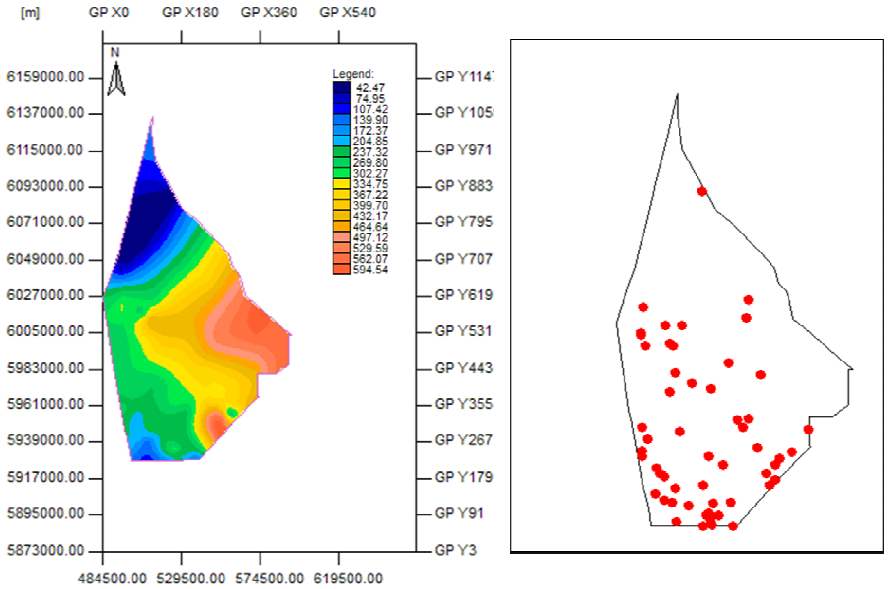

Figure 4: The wells used for to generate a thickness map of the Rotliegend and the generated map.

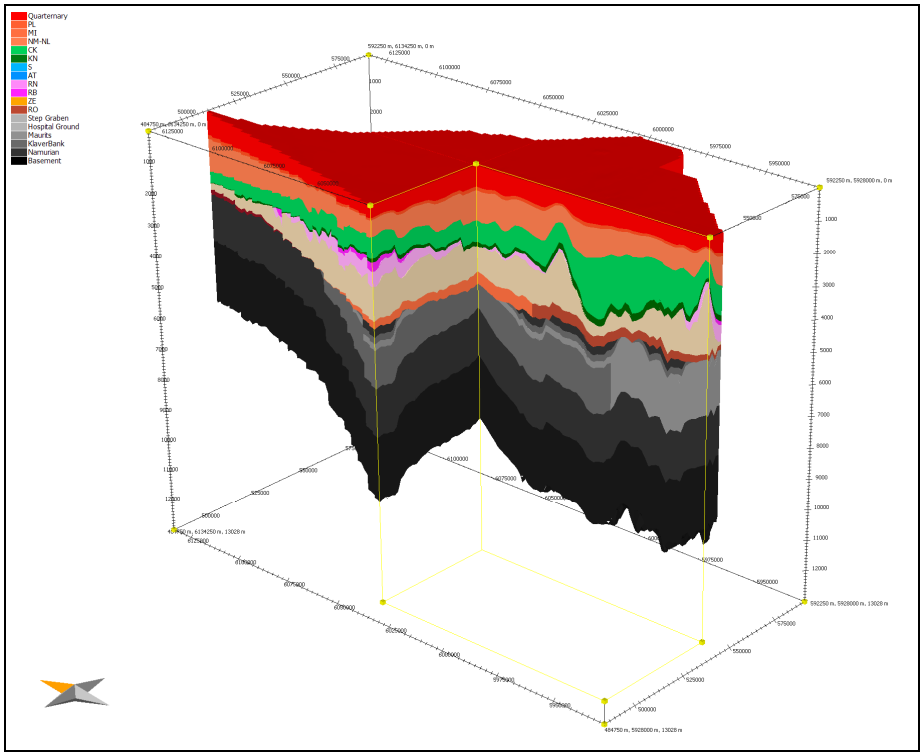

Figure 5: Present-day 3D geometrical model of the Cleaver Bank High.

The Carboniferous section in the model is constructed based on a subcrop map of the Carboniferous formations (Figure. 6). The subcrop map is based on well and biostratigraphic data (Kombrink et al., 2010). Based on well data and stratigraphical and palaeogeographical concepts, depositional thicknesses have been assigned to the formations. Depositional thicknesses of 300, 200 and 200 m are given to the Step Graben, the Hospital Ground and the Maurits formations respectively. The Klaverbank

Formation is given a depositional thickness that varies between 1500 m in the south to 1000 m in the north of the study area (Figure 7).

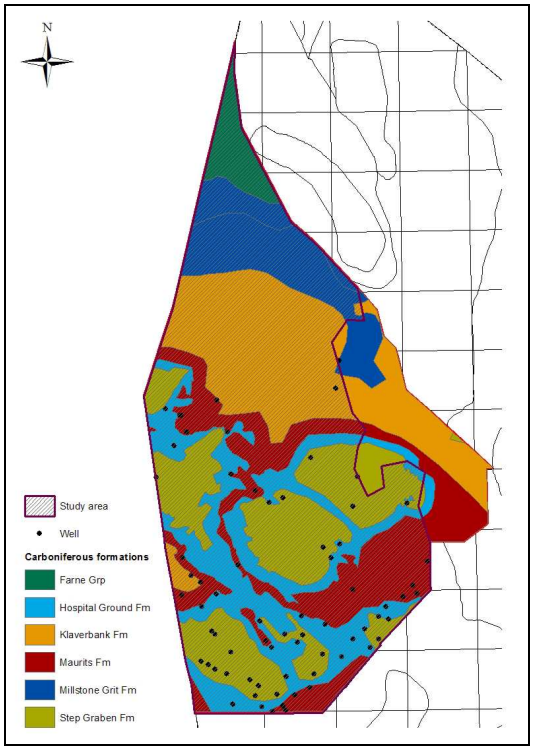

Figure 6: Subcrop map of the Carboniferous formations in the NCP-2D area (modified after Kombrink et al., 2010).

The subcrop map shows that in the northern part of the study area the Namurian and Westphalian succession (Millstone Grit Formation) have been eroded. The Dinantian Farne Group subcrops directly below the top Carboniferous (Figure 6). The Namurian and the Dinantian are given depositional thicknesses of 500 m and 1000 m respectively. Both layers are combined in the model in a single layer named the Pre-Westphalian layer with a total depositional thickness of 1500 m. Two lithofacies are assigned to the Pre-Westphalian layer in the model. Most of the Pre-Westphalian is assigned a deep marine facies which reflects the Namurian facies. In the northern part of the study area, the Pre-Westphalian layer is assigned a more fluvial and deltaic facies. This reflects the facies of the Dinantian Group (Gerling et al., 1999; Kombrink, 2008).

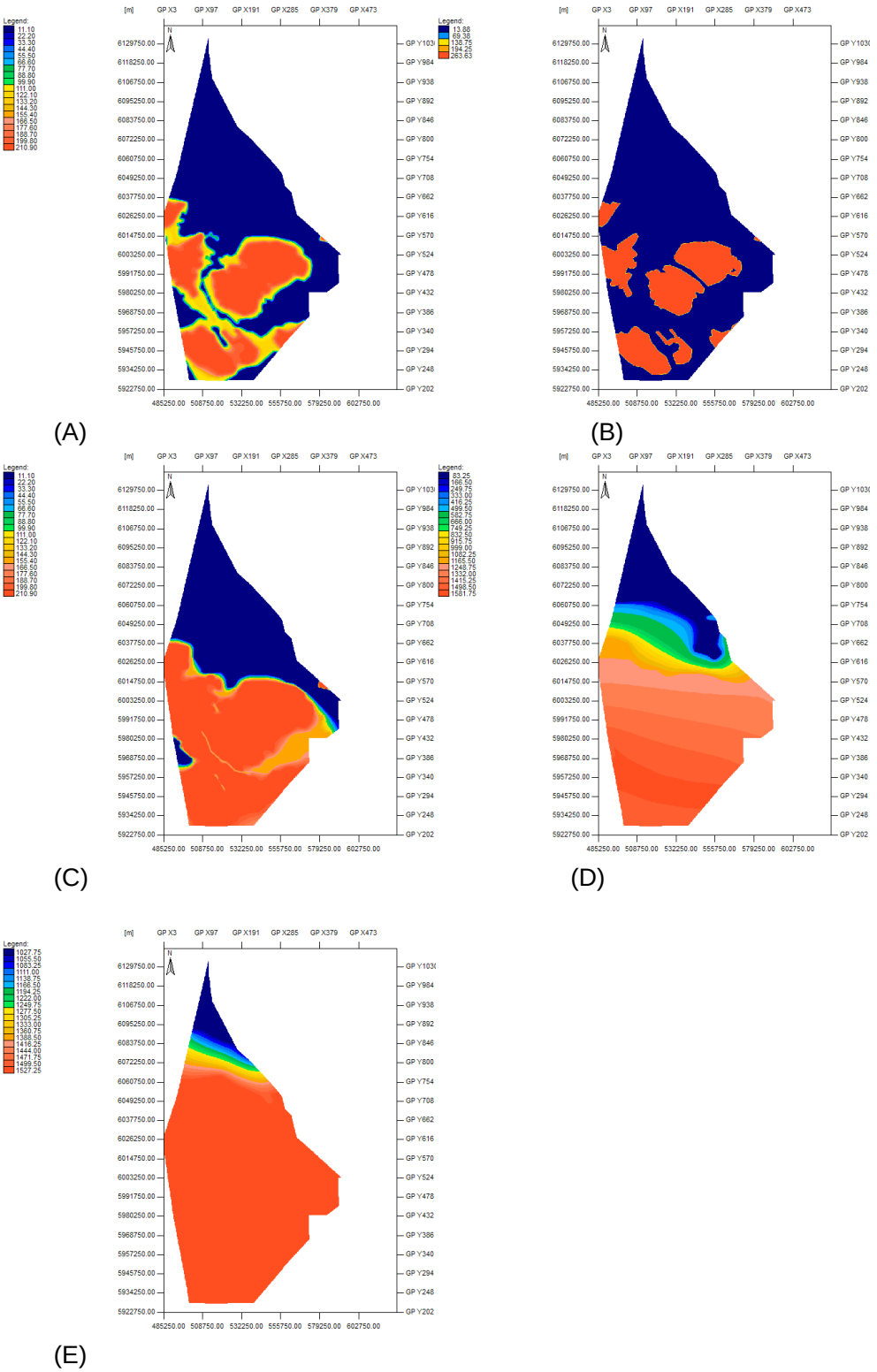

Figure 7: Thickness maps of Carboniferous layers. A: Step Graben, B: Hospital Ground, C: Maurits, D: Klaverbank, E: Pre-Westphalian.

2.5 Input: Properties

Lithology: The assigned lithology for each of the layers is based on the generalized description of the lithology of that formation-unit as described by Van Adrichem Boogaert and Kouwe (1993-1997). Facies variations are taken into account for three layers; the Rotliegend, the Klaverbank and the pre-Wesphalian formations (Figure 8). Based on well observations, facies maps are created to include lateral facies changes for these formations (Table 1).

Table 1. Layers and assigned lithological composition used in the model. Note the facies assigned to the Rotliegend Group, the Kalverbank Formation and the Namurian Formation.

Layer			Deposition Age [Ma]		Erosion Age [Ma]		Lithology
			From	To	From	To	Facies
1		***Quaternary***	***2.5***	***0***	***0***	***0***	75% Shale_25% Sand
2		***Pliocene***	***5.33***	***2.5***	***0***	***0***	50% Shale_50% Sand
3		***Miocene***	***20.1***	***5.33***	***0***	***0***	50% Shale_50% Sand
4		***Middle and Lower North Sea Group***	***56.8***	***28***	***0***	***0***	90% Shale_10% Sand
5		***Chalk***	***99.1***	***61.7***	***0***	***0***	100% Chalk
6		***Rijnland Group***	***124***	***99.1***	***0***	***0***	75% Shale_25% Silt
7		***Schieland Group***	***153.87***	***140.7***	***0***	***0***	75% Shale_25% Silt
8		***Altena Group***	***203.7***	***173***	***173***	***170***	75% Shale_25% Silt
9		***Upper Germanic Trias Group***	***246.2***	***203.7***	***170***	***165***	75% Shale_25% Silt
10		***Lower Germanic Trais Group***	***251***	***246.2***	***165***	***153.87***	75% Shale_25% Silt
11		***Zechstein Group***	***258***	***251***	***0***	***0***	100% Salt
12		***Rotliegend Group***	***263.99***	***258***	***0***	***0***	
		Rotliegend Group- North	***263.99***	***258***	***0***	***0***	90% Shale_10% Sand
		Rotliegend Group- South	***263.99***	***258***	***0***	***0***	95% Shale_5% Sand
		Rotliegend Group- Middle	***263.99***	***258***	***0***	***0***	80% Shale_50% Salt
13		***Step Graben***	***308.7***	***307***	***305***	***300***	50% Shale_50% Sand
14		***Hospital Ground***	***311***	***308.7***	***300***	***290***	50% Shale_50% Sand
15		***Maurits Formation***	***312***	***311***	***290***	***280***	80% Shale_15% Sand_5% Coal
16		***Klaverbank Formation***	***315.3***	***312***	***280***	***270***	
		Klaverbank Formation-North	***315.3***	***312***	***280***	***270***	80% Sand_20% Shale
		Klaverbank Formation-South	***315.3***	***312***	***280***	***270***	48%Shale_25%Sand_25% Silt_2% Coal
		Pre-Westphalian	***326.5***	***315.3***	***0***	***0***	60% Shale_40% Sand
		Pre-Westphalian–South (Namurian)	***326.5***	***315.3***	***0***	***0***	60% Shale_40% Sand
17		*Pre-Westphalian -North (Dinantian)*	***326.5***	***315.3***	***0***	***0***	50% Shale_50% Sand
18		***Basement***	***340***	***326.5***	***0***	***0***	Basement

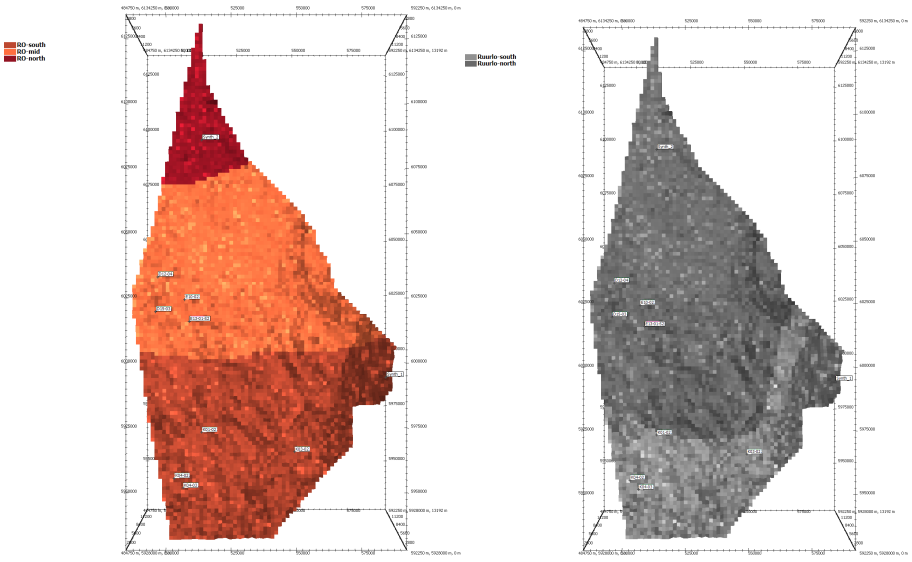

Figure 8: Facies distribution for the Rotliegend group and the Klaverbank Formation.

Source rock properties: The major source rock intervals in the model are the Carboniferous Coal Measures of the Limburg Group. These include the Klaverbank and Maurits coal bearing formations. Both formations are defined as source rock of kerogen type III. For the Klaverbank Formation, the properties varied following the lateral facies distribution in the area. The Pre-Westphalian layer is defined in the model as source rock with two facies. Two source rock types are assigned to the this layer to reflect the two facies. The northern part of the layer, where the Namurian is eroded and the Dinantian subcrops, is defined as a source rock of type III. The rest of the layer is defied a source rock type II which represents the Namurian facies. The original TOC and HI values used in the modelling are estimated from measured data from surrounding areas in our in-house database and published sources (e.g., Gerling et al., 1999; Van Balen et al., 2000; Pletsche et al., 2010). Source rock properties of these intervals are shown in table 2

Thermal properties: The thermal conductivity values for the lithologies were defined based on a default thermal conductivity model (the Sekiguchi Model) (PetroMod 11, IES Schlumberger). The radiogenic heat production is calculated for the rock matrixes for each of the lithologies. The calculation of the radiogenic heat is based on assumed default concentrations of certain minerals (Uranium, Thorium and Potassium) in the major lithological units. The Rybach equation is used to derive the heat production from the concentrations of the minerals. For mixed lithologies, the heat production for various lithological components was arithmetically averaged.

Mechanical Compaction: For all major lithologies, a default compaction model was applied. The model is based on the Hydrostatic Athy's law Model where the porosity versus depth curve is theoretical curve that assumes a hydrostatic pressure and a uniform lithological column. The solid rock is incompressible. Salt is impermeable (k = 10^-16 mD).

Table 2. Average source rock parameters used for simulating timing of hydrocarbon generation.

Source rock	Kerogen type	TOC Input PM (wt%)	HI input PM (mgHC/gTOC)
Maurits	Type III	4.0	200
Klaverbank-North	Type III	1.00	100
Klaverbank-South	Type III	3.0	100
Pre- Westphalian-North (Dinantian)	Type III	2.0	200
Pre-Westphalian - South (Namurian)	Type II	2.0	200

Pore water/formation water properties: In the model the pore water is of constant density that is the density of the water is independent of changes in temperature and salinity. The water is incompressible.

2.6 Erosion Input

The geological evolution of the area includes the two main phases of erosion, namely the Saalian and the Mid-Kimmerian to Late-Kimmerian, as well as additional periods of non-deposition (Table 1). The amount of eroded material is estimated for each erosional period using regional and stratigraphic information from well and seismic data.
Carboniferous deposits underwent strong uplift and erosion during the Latest Carboniferous and Early Permian (Saalian uplift). Erosional thicknesses are calculated based on the subcrop map and the assumed depositional thicknesses (Figures 6).

The platforms in the NCP-2D area were again uplifted during the Late Jurassic (Mid– and Late Kimmerian erosion). The movement caused deep erosion and complete removal of the Lower to Middle Jurassic sediments as well as parts of the Triassic sediments. The eroded thicknesses of the Triassic and Jurassic layers are calculated from assumed uniform depositional thickness. Depositional thicknesses are assumed based on well data and regional stratigraphic correlations.

The erosion maps of the Altena Group (AT), the Upper Germanic Trias Group (RN) and the Lower Germanic Trias Group (RB), are calculated assuming depositional thicknesses of 200 m, 400 m and 500 m respectively (Figure. 9).

2.7 Boundary conditions

Paleo water depths: Detailed paleo water depth (PWD) values were used in the modelling. The PWD curve was compiled based on literature research for some time intervals as well as detailed investigation by the Geobiology department at TNO for some specific intervals. The paleo water depths were allowed to vary in time but were kept constant over the entire area at a certain time (Figure 10).

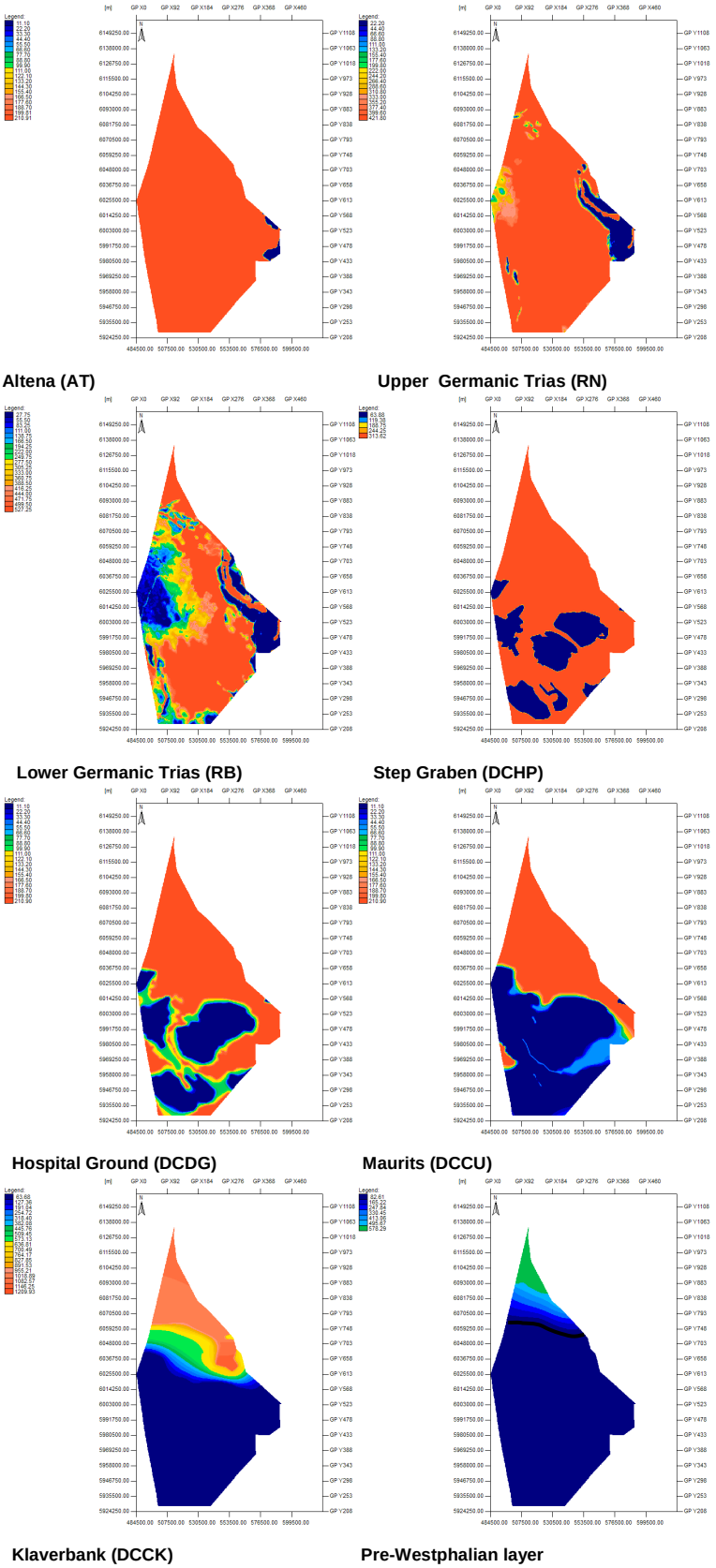

Figure 9: Erosion maps of the main eroded units in the study area as introduced to the model.

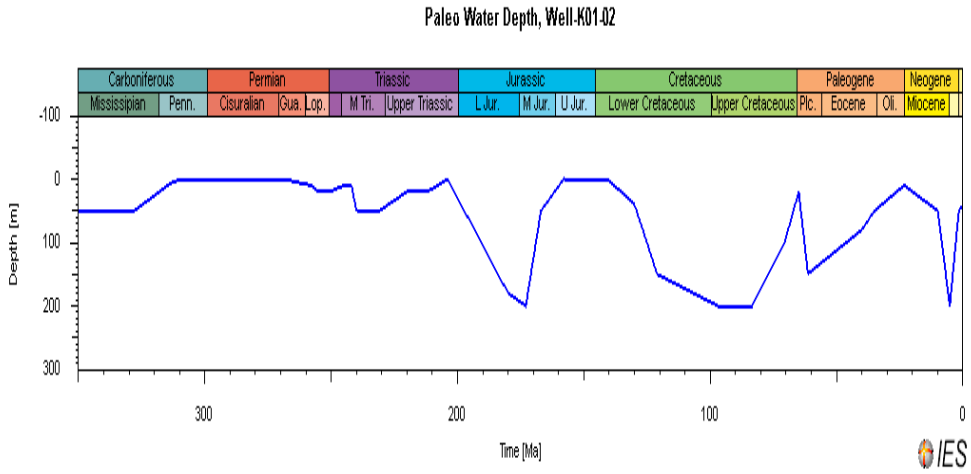

Figure 10: Detailed Paleo Water Depth curve based on a combination of published data and Geobiologic analysis.

Paleo surface temperature: The paleo surface temperature at the sediment water interface was calculated with an integrated Petromod tool that takes into account the paleo water depth and the evolution of ocean surface temperatures through time depending on paleolatitude of the area. For the Tertiary and Quaternary history of SWIT's more detailed temperature boundary conditions were reconstructed. The temperatures at a certain time are kept constant over the entire area (Figure 11) (Verwij at al., 2010).

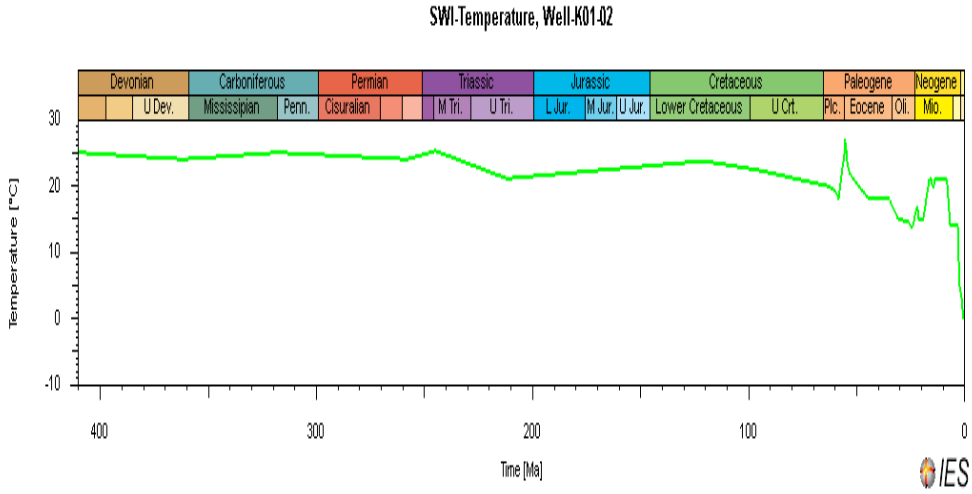

Figure 11: Detailed Paleo Surface Water Interface Temperature curve based on a combination of published data and Geobioligic analysis.

Paleo basal heat flow: Basal heat flow was modelled in the area using the in-house developed 1D tectonic heat flow modelling tool PetroProb. The tool uses the sedimentation, uplift and erosion history for single wells to predict the evolution of the basal heat flow in that well. PetroProb takes into account the tectonic evolution of the basin and requires a user-defined model of the lithosphere. Uncertainties in the input parameters are taken into account during the calculations and as a result the modelled heat flows are expressed in a probabilistic way. The models are calibrated to measured

temperatures and vitrinite reflectance data from the well and the heat flow model that gives the best fit is selected (Van Wees et al., 2009)
Based on the stratigraphy of the area, two wells were selected for heat flow modelling. Well E10-02 was used to model the heat flow in the northern part of the NCP-2D area and well K01-02 was used to model the heat flow in the southern part of the area (Figure 12). More details about the modelling the basal heat flow and the applied parameters are presented in chapter 3.

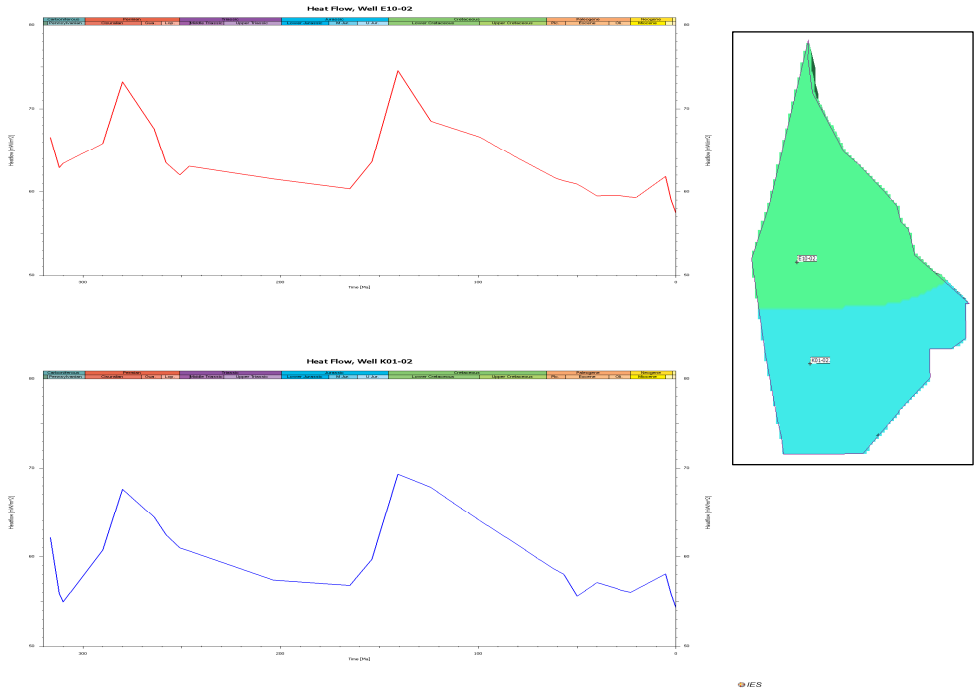

Figure 12: Basal heat flow used in modelling the area. Two wells were used to calculates the tectonic heat flow, E10-02 for the northern part and K01-02 for the southern part.

2.8 Basin modelling: Default set-ups, calibration

The PetroMod programme provides an extensive suit of default set-ups. Default set-ups that are used in the simulations concern the lithology and mixed lithology and their associated default properties. These include thermal conductivity, radiogenic heat production, heat capacity as well as default mechanical compaction equations and default porosity-permeability relations.
The thermal conductivity values of the lithologies are defined based on a default thermal conductivity model (the Sekiguchi Model; PetroMod 11). The radiogenic heat production is calculated for the rock matrices for each of the lithologies. For all major lithologies, a default compaction model is applied. The compaction model is based on the Hydrostatic Athy's law Model where the porosity versus depth curve is theoretical curve that assumes a hydrostatic pressure and a uniform lithological column (Annex 1 provides more detailed information).

Measured porosities and permeabilities provided the basis for selecting the proper compaction and porosity-permeability relations. Measured present day temperature and vitrinite reflectance data are used to calibrate the 1D and later the 3D input model.

The maturity modelling is based on the Sweeney and Burnham (1990) kinetic model. The calculations of the transformation ratios for the assigned source rock intervals are based on the Pepper and Corvi (1995) TII and TIII hydrocarbon generation kinetics. The implemented generation kinetics depends on the facies assigned. The Pepper and Corvi (1995) TII kinetics is used for the southern and central part of the Base Carboniferous layer (the Namurian facies) The Pepper and Corvi (1995) TIII is used for the Westphalian formations (Maurits, Klaverbank) and the northern part of the Base Carboniferous layer (the Dinantian facies).

The input geological model is without faults and assumes open fluid flow boundaries. The 3D simulations of temperature and maturity are run assuming hydrostatic conditions and only conductive heat flow is assumed in the model. Salt movement and, as a consequence, the thermal effect related to it are not considered in the modelling. The present-day thickness of the Zechstein Formation in the platform area does not indicate strong salt tectonics during the evolution of the basin.

3 Basal Heat Flow modelling: Input parameters and modelling results

Basal heat flow is an essential boundary condition for maturity modelling. Usually a constant heat flow is used as an input where a single value is assumed for the whole basin and during the development history of the basin. TNO, however, uses a modelling tool (PetroProb) to calculate the basal heat flow based on the tectonic evolution of the basin. The modelling result is a heat flow model that varies over time expressed in a probabilistic way that takes the uncertainties in the inputs into account.
Although PetroProb is able to generate basal heat flow maps, single wells are often used as inputs and the resulting heat flow models are usually used for the whole modelling area. For the NCP-2D area however, we use two wells to model the heat flow in the area. The areas are then divided into two areas and the basal heat flow models are assigned to each of them.

3.1 Selection of wells

Judging from the stratigraphy of the area, it was decided to model two wells for heat flow instead of only one. A cross section in the area shows that in southern part of the area (where well K01-02 is located) the Chalk Group is thicker than in the northern part of the area (where well E10-02 is located). Moreover, while the Lower Germanic Trias Group is totally absent in the southern part of the area, its thickness increases towards the north (Figure 13).
Such a pronounced difference in the stratigraphy between these areas would have an important effect on the burial history and the tectonic subsidence of the areas and thus on the evolution of the basal heat flow (Figure 13). The selection of the wells K01-02 and E10-02 was based on several criteria, such as: the depth of the well, absence of faults and the availability and the quality of calibration data such as measured temperature and vitrinite reflectance.

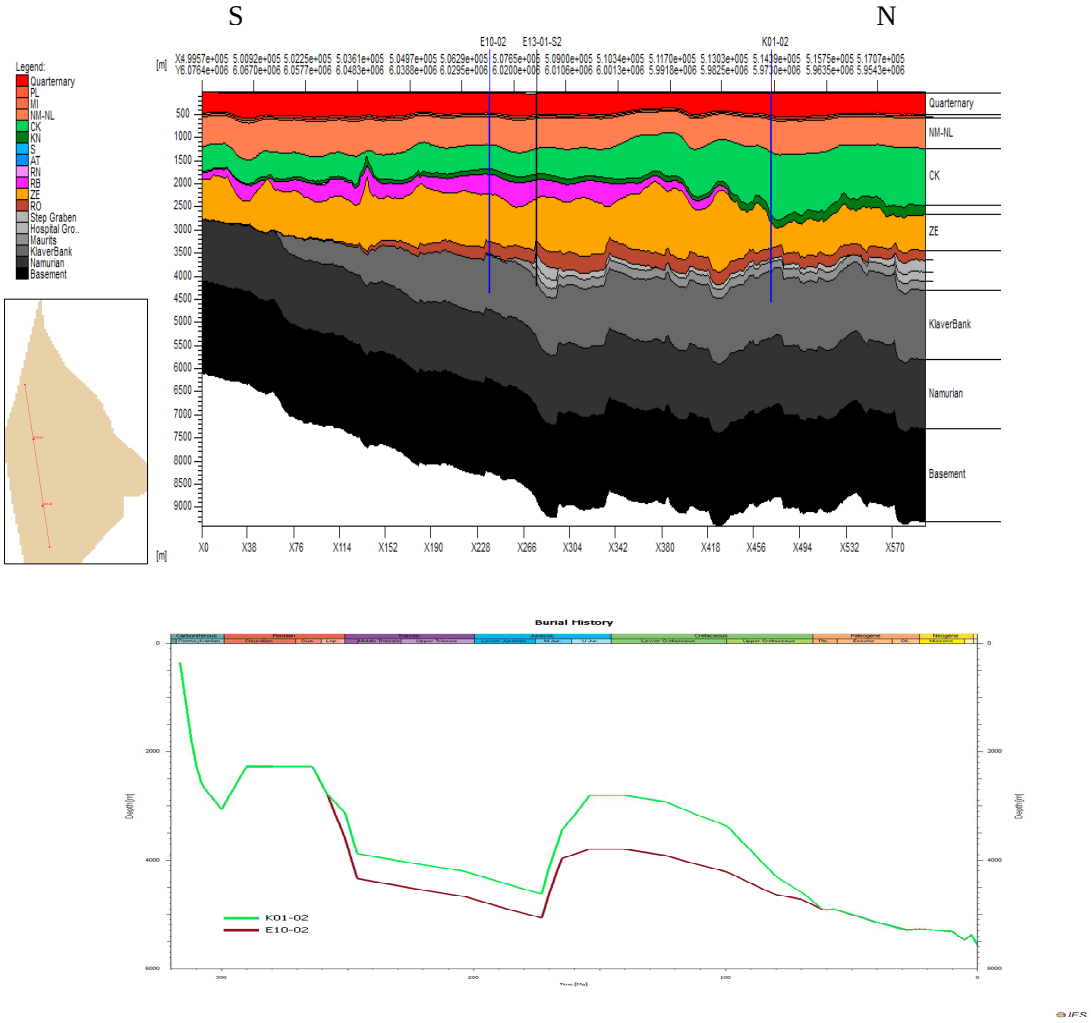

Figure 13: Cross section though the study area showing the stratigraphical variations that led to our well selection for heat flow modelling (Top). The burial history of the selected wells is shown (Below).

3.1.1 Heat flow modelling Well E10-02

- Input Data

A more refined and detailed stratigraphy was used for the 1 D heat flow modelling than in the 3D maturity modelling. The well penetrates the Rotliegend (RO) Group as well as the Carboniferous and the thicknesses used in the modelling are the observed ones (Figure 14). As in the 3D modelling, two major erosion phases are introduced, the Saalian phase which removed the upper part of the Carboniferous, and the Mid –Late Kimmerian phase that eroded the Jurassic and partly the Triassic (Figure 14).

Layer	Top [m]	Base [m]	Thick. [m]	Eroded [m]	Depo. from [Ma]	Depo. to [Ma]	Eroded from [Ma]	Eroded to [Ma]	Lithology
NUMS	30	343	313		2.59	0.00			Sand/Shale_75
NUOT	343	496	153		5.33	2.59			Sand/Shale_75
NUBA	496	511	15		20.43	14.80			Sand/Shale_75
NM	511	572	61		38.60	30.40			Sand/Shale_75
NLFFB	572	606	34		44.70	42.10			Shale (typical)_1
NLFFM	606	658	52		47.30	44.70			Shale/Marl_50
NLFFY	658	1172	514		50.00	47.30			Shale (typical)_1
NLFFT	1172	1186	14		56.50	50.00			Shale/Tuff_50
NLLFC	1186	1224	38		60.50	56.50			Shale (typical)_1
CKGR	1224	1782	558		92.90	61.70			Chalk (typical)
CKTX	1782	1823	41		99.10	92.90			Chalk/Marl_75
KNGLU	1823	1851	28		104.80	99.10			Marl_100
KNGLM	1851	1866	14		112.90	104.80			Shale (typical)_1
KNGLL	1866	1879	14		121.80	112.90			Marl/Shale_75
KNNCM	1879	1891	12		124.00	121.80			Marl/Shale_75
KNNCK	1891	1927	36		130.00	124.30			Marl/Shale_75
KNNCM	1927	1954	27		132.00	130.00			Marl/Shale_75
AT-erosion	1954	1954	0	200	203.60	163.40	158.00	154.00	Marl/Shale_75
RN-erosion	1954	1954	0	900	246.20	203.60	154.00	141.00	Marl/Shale_75
RB-erosion	1954	1954	0	100	247.60	247.00	141.00	136.00	Marl/Shale_75
RBMDL	1954	1969	15		247.80	247.60			Sand/Shale_75
RBMVC	1969	1992	23		248.60	247.80			Shale/Silt/Sand_33/33/34
RBMVL	1992	2050	58		249.00	248.60			Sandstone_100
RBSHR	2050	2263	213		250.00	249.00			Shale/Silt/Lime_50/25/25
RBSHM	2263	2431	168		251.00	250.00			Shale/Silt_75
ZEUC	2431	2436	5		251.60	251.00			Shale (typical)_1
ZEZ4R	2436	2440	4		252.80	252.60			Shale/Anhy_75
ZESAL	2440	3552	1112		255.70	252.80			Salt/Shale/Dolo_85/10/5
ZEZ2C	3552	3564	12		256.40	255.70			Lime/Dolo_75
ZEZ1A	3564	3590	26		257.40	257.20			Anhydrite_100
ZEZ1C	3590	3594	4		257.80	257.40			Limestone_100
ZEZ1K	3594	3595	1		258.00	257.80			Shale (typical)_1
ROCLU	3595	3703	108		259.00	258.00			Shale/Silt_50
ROCLE	3703	3874	171		265.00	259.00			Silt/Shale/Salt/Anhy_30/30/20/20
DC-erosion	3874	3874	0	400	311.00	290.00	290.00	280.00	Silt/Shale/Salt/Anhy_30/30/20/20
DCCU	3874	3953	79		312.30	311.00			Shale/Sand/Coal_80/15/5
DCCKB	3953	4297	344		313.10	312.30			Shale/Silt/Sand/Coal_48/25/25/02
DCCKM	4297	4380	83		314.00	313.10			Shale/Sand/Coal_78/20/2
Basement	4380	4500	120		500.00	314.00			BASEMENT

Figure 14: The stratigraphy and litholgoy used as input for modelling heat flow in well E10-02. The major erosion phases are indicated in the red frames.

For the 1D heat flow modelling we assumed an eroded Upper Carboniferous of 400 m. For the Altena (AT), we assumed an eroded thickness of 200 m and for the Upper Germanic Trias (RN) and Lower Germanic Trias (RB) 900 m and 100 m respectively. The erosion values were chosen so that the modelled heat flow would give the best fit with the measured values of temperature and vitrinite reflectance. The assumed erosion values at this stage are based on the refined and detailed models on basal heat flow modelling. This means that the values are subject to more constraining and refinement later when the 3D maturity model is constructed and when more wells in the area are used for calibrating the 3D model (see below).

The paleo water depth values used in heat flow modelling are based on the latest data available from the TNO Geobiology department in combination with published data (Figure 15). The sediment water interface temperatures (SWIT) are also based on the latest analyses by the Geobiology department as well as published data (Figure 13). These data were derived from surface water interface temperatures that were corrected for paleo water depths. For heat flow modelling, the Surface Water Interface Temperature (SWIT) and the Paleo Water Depth (PWD) that were used as inputs in PetroProb were slightly modified so that it is consistent with the age inputs in PetroProb. This included using only discrete and specific time intervals from the details curves for PWD and SWIT that coincide with the input ages for the wells.

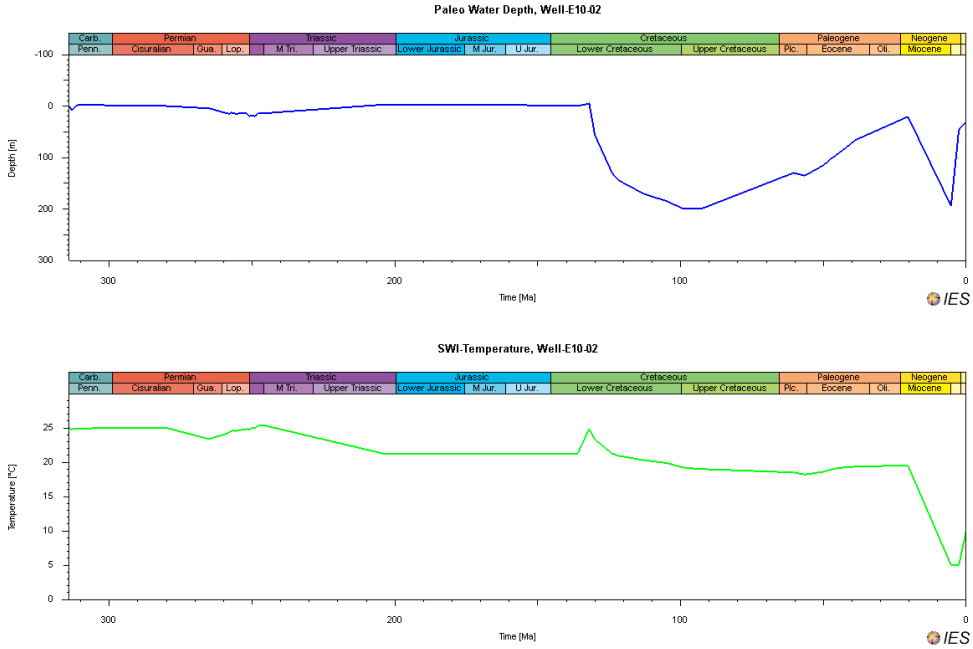

Figure 15: Paleo water depth values (top) and sediment water interface temperature (below) used for heat flow modelling in Well E10-02 in PetroProb. The data here are plotted in PetroMod for illustration purposes.

Other parameters used in PetroProb for heat flow modelling in this well, such as decompaction parameters, sediment thermal parameters, lithosphere parameters, are shown in Annex 2 .

One of the most important parameters in basal heat flow modelling is the initial tectonic model that describes the major tectonic events. This input defines the major phases of tectonic stretching and allows the user to quantify the stretching magnitude for both the crust (a) as well as the upper mantel (b). This allows PetroProb to constrain the inversion of the tectonic subsidence curve which is derived from the backstripped burial history. A variety of tectonic scenarios can be included in order to describe the tectonic history of the basin. The tectonic steps introduced to PetroProb to describe this well and therefore calculate the heat flow are shown in Annex 2.

Major tectonic activities and events implemented in the model included both uplift and erosion phases during the Saalian which is defined from 290 Ma to 280 Ma, and the Mid and Late Kimmerian defined from 158 Ma to 136 Ma. The first erosion phase was identified as a thermal uplifting event followed by a thermal relaxation that provided accommodation for the sediments later. This phase is thought to be related to the Early Permian regional thermal uplift. Therefore, we adopt a non-uniform tectonic model where the sub-crustal lithosphere undergoes more stretching than the crustal lithosphere which remains stable. This is expressed in PetroProb as (a) = 1 and (b) = free (see Annex 2).

For the Mid-Late Kimmerian phase, we chose a similar tectonic model where thermal doming is assumed. However, the regional tectonic settings that prevailed during Mid Jurassic forces were different from that dominated during the Early Permian. The Early Permian thermal uplift is though not to be associated with any substantial regional stretching and the crust did not undergo and major stretching (Van Wees et al., 2000) . For this reason the crust's stretching factor was set equal to 1. In the Jurassic however, the general regional setting was extensional and the thermal doming was most likely associated (or immediately followed) by a crustal stretching. Based on that, it is

possible to assume that during the Mid-Late Kimmerian event stretching took place in the crustal as well as the sub-crustal lithosphere. Since thermal uplift dominated and some volcanism associated with this event was also observed we assumed that the sub-crustal stretching factor was more dominant and thus has a higher value. This would be translated in our modelling as a model where (a) is set "free" (varies independently) and (b) is set to a value that is higher than 1. The advantage of such a mode is that it counts for a crustal stretching (extensional settings) as well as a thermal uplift and underplating that results in erosion at the same time.
For the sake of simplicity, we adopted a model where the crustal stretching (a) is set constant to 1, and the sub-crustal stretching is set "free". This is expressed in PetroProb as a) = 1 and (b) = free (see Annex 2). Some test models that were carried out to evaluate and compare different modelling parameters indicated that the resulted heat flow for this case would not vary dramatically when some extensional component for the crust is incorporated in the model.

- Modelled Basement Heat Flow Well E10-02

The modelled heat flows were calibrated with temperature and vitrinite reflectance data (see Annex 3). The modelled tectonic heat flow for his well is shown in figure 16. The figure shows a good fit between the observed tectonic subsidence and the modelled one. The calibration results of this well using the modelled heat flow are shown in figure 15. The comparison between the modelled temperatures and vitrinite reflectance and the measured data shows a good fit. Further adjustments on the erosion amounts for even a better fit can be done on a larger scale when the 3D model for the whole area is created. For the purpose of generating heat flow models we consider this fit is an acceptable one and the effect of the erosion load will be discussed when the 3D model is established.
The resulted basal heat flow was used for the whole northern part of the NCP-2D area.

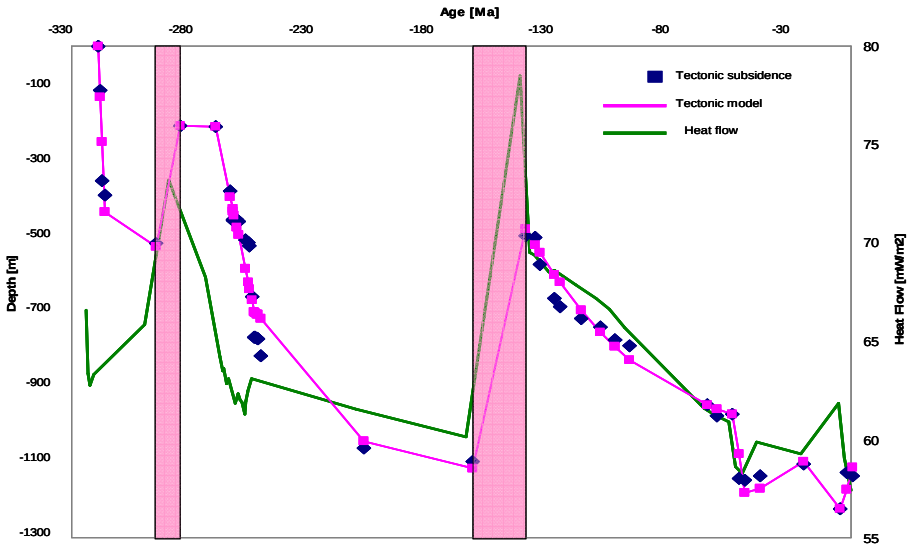

Figure 16: Basement heat flow modelled in PetroProb and calibrated with measured data (Well 10-02). Both observed and modelled tectonic subsidence are also shown.

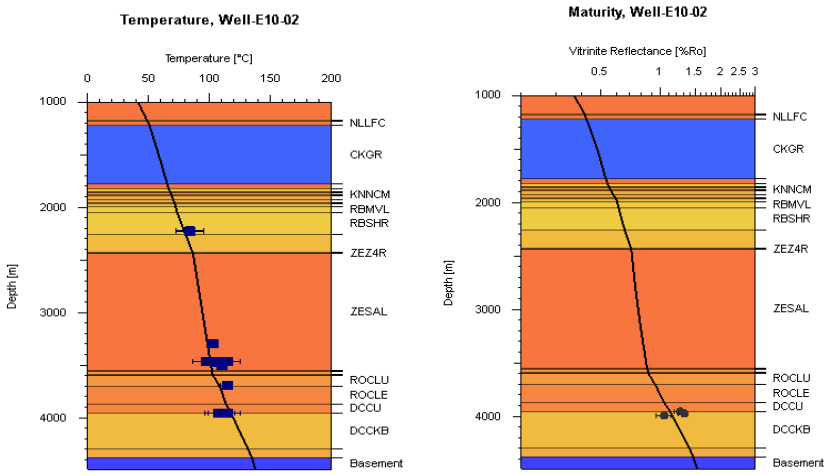

Figure 17: Results of calibration between calculated Temperature (Left) and Maturity (Right) and measured data (Well E10-02).

The modelled heat flow at this well shows two major heat flow peaks that are associated with the major erosion phases. Since the erosion phases are defined in the model as uplift events associated with thermal uplift, a major heat flow peak is observed during these phases. The heat peak observed at these phases is not only related to the amount of erosion, but also to the depth of the magmatic event, the thickness of the underplating as well as its temperature. In this well, the calculated present-day heat flow is about 68 mW/m2, while the highest peak is reached during the Mid Kimmerian phase when the heat flow reached a value of around 76 mW/m2.

3.1.2 Heat flow modelling Well K01-02

- Input Data

A more detailed stratigraphy was used for the 1D heat flow modelling compared with the one used in the 3D maturity modelling. Both the Rotliegend (RO) and the Carboniferous (DC) are penetrated in the well. The thicknesses used in the modelling are the observed ones (Figure 16). As in the 3D modelling, two major erosion phases are introduced, the Saalian phase which removed the upper part of the Carboniferous, and the Mid-Late Kimmerian phase that eroded the Jurassic and partly the Triassic (Figure 18).

For the 1D heat flow modelling in this wells we assumed an eroded Upper Carboniferous of 400 m. For the Altena (AT), we assumed 200 m and 900 m and 500 m for the Upper Germanic Trias (RN) and Lower Germanic Trias (RB) respectively. The erosion values were chosen so that the modelled heat flow would give the best fit with the measured temperatures and vitrinite reflectance. The assumed erosion values at this stage are based on the refined and detailed models on basal heat flow modelling. This means that the values are subject to more constraining and refinement later when the 3D maturity model is constructed and when more wells in the area are used for calibrating the 3D model (see below).

Layer	Top [m]	Base [m]	Thick. [m]	Eroded [m]	Depo. from [Ma]	Depo. to [Ma]	Eroded from [Ma]	Eroded to [Ma]	Lithology
NUMS	30	250	220		2.59	0.00			Sand/Shale_50
NUOT	250	450	200		5.33	2.59			Sand/Shale_50
NUBA	450	556	106		24.00	5.33			Sand/Shale_50
NM	556	636	80		35.40	24.00			Sand/Shale_50
NLFFB	636	676	40		42.00	37.90			Shale_LOw Radio_Nor_1
NLFFM	676	734	58		50.00	42.00			Shale/Marl_50
NLFFY	734	1281	547		54.00	50.00			Shale_LOw Radio_Nor_1
NLFFT	1281	1304	23		55.10	54.00			Shale_LOw Radio_Nor_1
NLLFC	1304	1356	52		60.50	56.50			Shale_LOw Radio_Nor_1
CKEK	1356	1405	49		65.00	60.50			Limestone_100
CKGR	1405	2664	1259		90.40	65.00			Limestone_100
CKTX	2664	2709	45		97.00	90.40			Lime/Marl_75
KNGLU	2709	2730	21		104.80	99.10			Marl_100
KNGLM	2730	2744	14		112.90	104.80			Shale (typical)_1
KNGLL	2744	2750	5		121.80	112.90			Marl/Shale_75
KNNC	2750	2874	124		138.60	130.00			Shale (typical)_1
KNNSF	2874	2882	8		138.80	138.60			Sandstone_100
AT-erosion	2882	2882	0	200	203.60	163.40	158.00	154.00	Sandstone_100
RN-erosion	2882	2882	0	900	245.00	213.60	154.00	145.00	Sandstone_100
RB-erosion	2882	2882	0	500	251.00	247.20	145.00	140.00	Sandstone_100
ZECP	2882	2889	7		252.60	252.00			Anhy/Shale_50
ZEZ4R	2889	2904	15		252.80	252.60			Shale/Anhy_75
ZEZ3H	2904	2937	33		254.00	252.80			Salt_100
ZEZ3A	2937	2984	47		254.10	254.00			Anhy/Dolo/Shale_80/10/10
ZEZ3C	2984	2986	2		254.30	254.10			Dolomite_100
ZEZ3G	2986	2987	1		254.50	254.30			Shale (typical)_1
ZEZ2T	2987	2989	2		254.60	254.50			Anhydrite_100
ZEZ2H	2989	3352	364		255.60	254.60			Salt_100
ZEZ2A	3352	3356	3		255.70	255.60			Anhydrite_100
ZEZ2C	3356	3365	9		256.40	255.70			Lime/Dolo_75
ZEZ1W	3365	3381	16		257.40	256.40			Anhydrite_100
ZEZ1C	3381	3390	9		257.80	257.40			Limestone_100
ZEZ1K	3390	3391	0		258.00	257.80			Shale (typical)_1
ROCL	3391	3629	239		267.50	258.00			Shale/Sand_75
Dc-Erosion	3629	3629	0	400	311.00	290.00	290.00	280.00	Shale/Sand_75
DCCU	3629	3852	223		312.30	311.00			Shale/Sand/Coal_80/15/5
DCCKB	3852	4263	411		313.10	312.30			Shale/Silt/Sand/Coal_48/25/25/02
DCCKM	4263	4551	288		314.00	313.10			Shale/Sand/Coal_78/20/2
Basement	4551	5000	449		500.00	314.00			BASEMENT
						500.00			

Figure 18: The stratigraphy and lithology used as input for modelling heat flow in well K01-02. The major erosion phases are indicated in the red frames.

The paleo water depth values and the sediment water interface temperatures (SWIT) used in heat flow modelling are similar to those used in the previous well (Figure 15).
Other parameters used in PetroProb for heat flow modelling in this well, such as decompaction parameters, sediment thermal parameters, lithosphere parameters, are shown in Annex 2 . The tectonic model used for heat flow calculation is similar to the one used in the previous well (see above).

- Modelled Basement Heat Flow Well K01-02

The modelled heat flows were calibrated to temperature as well as vitrinite data (see Annex 3). The modelled tectonic heat flow for his well is shown in figure 19. The figure shows a good fit is achieved between the observed tectonic subsidence and the modelled one. The calibration results of this well using the modelled heat flow are shown in figure 19. The comparison between the modelled temperatures and the measured data shows a relatively good fit. The modelled vitrinite reflectance trend using this heat flow however results in higher values than the measured data. The trend of the modelled vitrinite reflectance is however similar to that of the measured data. Using different erosion amounts can have effect on the fitting of the vitrinite reflectance. Different erosion scenarios will be discussed when the 3D maturity model is calculated and the vitrinite reflectance data will then be compared to the modelled values. The modelled temperature data show a good fit with the measurements in this well. The resulted basal heat flow was used for the whole southern part of the NCP-2D area.

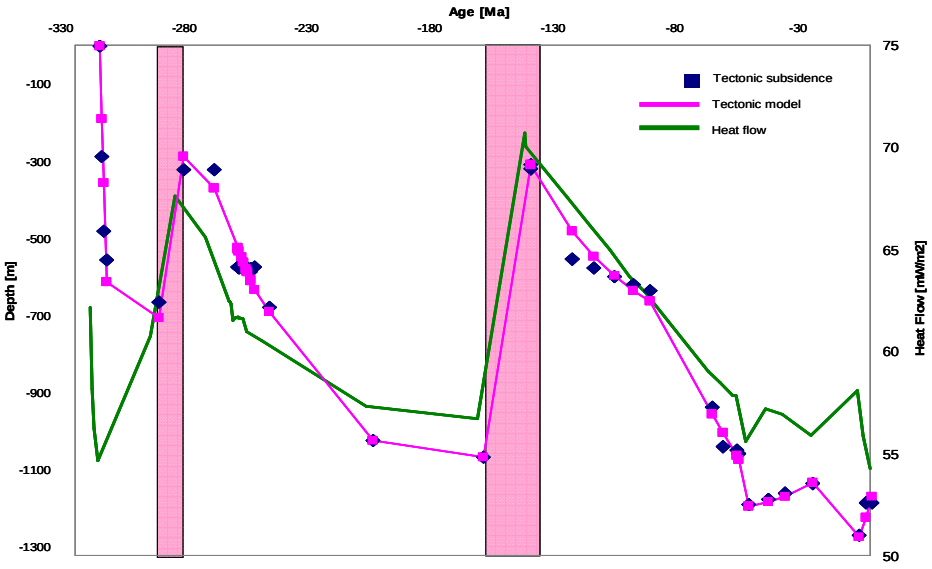

Figure 19: Basement heat flow modelled in PetroProb and calibrated with measured data at well K01-02 . Both observed and modelled tectonic subsidence are also shown.

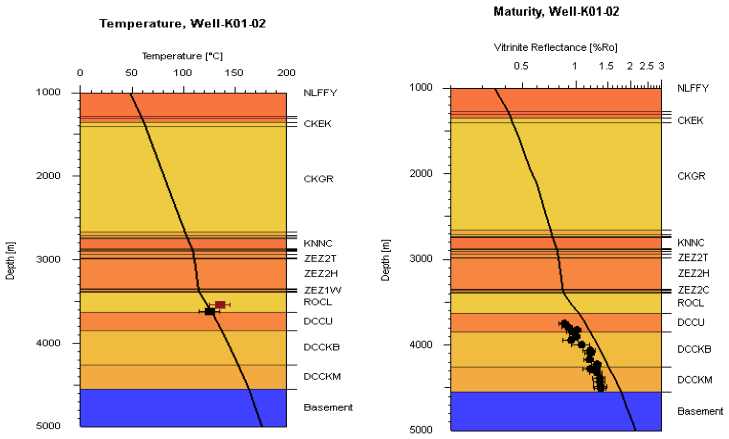

Figure 20: Results of calibration between calculated temperature (left) and maturity (right) and measured data using the modelled heat flow at well K01-02. While a good fit is achieved for the temperature, the vitrinite data seem to be difficult to fit.

The modelled heat flow at well K01-02 shows two major heat flow peak that are associated and related to the major erosion phases. Two major heat flow peaks are observed during these thermal uplift phases. The heat peak observed is not only related to the amount of erosion, but also to the depth of the magmatic event, the thickness of the under plating as well as its temperature. In this well, the present day heat flow is about 55 mW/m2, while the highest peak is reached during the Mid Kimmerian phase when the heat flow reached a value of around 70 mW/m2.

The modelled heat flow in this well is remarkably lower than that in well E10-02 in the northern part of the area (Figure 16). The differences between both wells i

s attributed to the differences in the lithostratigraphic columns in both wells as well as the tectonic evolution of both wells.

4 Modelling results: burial history, temperature, maturity

The simulations of the temperature and heat flow history started with a thermal model that is based on the default Petromod lithology-related thermal conductivities (Sekiguchi model), heat capacities and radiogenic heat production. Basal heat flow was modelled in two wells in the area and was used as bottom boundary condition (chapter 3). Basin assumptions for the modelling included zero heat flow across lateral boundaries, a transient heat flow through the sediments, and the history of sediment water interface temperatures. Note that Petromod simulations do not take the influence of fluid flow on thermal conditions in the basin into account.
Present-day temperatures and vitrinite reflectance measurements were available for calibration purposes (see below).
Data from nine wells are used for calibrating our 3D models (Table 3). The data (temperature and/or vitrinite reflectance) are compared to the modelled data at the location of the well in the 3D model. The calibration data of some of these wells are listed in Annex 3 .

Table 3: List of wells used for calibrating the 3D model.

Well Name	Surface X-Coordinate [m]	Surface Y-Coordinate [m]	Bottom-Hole X-Coordinate [m]	Bottom-Hole Y-Coordinate [m]	Start Elevation (KB or DF) [m]	Total Drill Depth [m]	True Vertical Depth [m]
D12-04	496979	6033580	496979	6033580	34	3914	3914
D15-03	496215	6019812	496215	6019812	35	4017	4016
E02-02	523748	6088759	523748	6088759	35	2647	2647
E10-02	507283	6024417	507283	6024417	41	4386	4386
E13-01-S2	509007	6016047	509007	6016047	47	4277	4266
K01-02	513888	5973416	513888	5973416	30	4586	4586
K03-02	549363	5965944	549363	5965944	39	4445	4443
K04-02	503321	5955721	503321	5955721	27	2580	2580
K04-03	506743	5952035	506743	5952035	41	3980	3980

4.1 Burial history

The burial history, as well as temperature and maturity history, in the NCP-2D area are discussed using representative 1D extractions of the 3D model at the location of three wells; E10-02 located on the Silverpit Platform, well K01-02 located on the Cleaver Bank Platform, well E02-02 located in the northern part of the study area and within the Elbow Spit Platform (ESP; Figure 21).

The burial histories (Figure 22) show two phases of rapid subsidence and sedimentation in the three platforms during the Late Carboniferous and Late Permian-Early Triassic (~ 270-245 Ma). Two uplift phases are also observed in the burial history of the wells during the Early Permian and Mid-Late Jurassic (~ 170-150 Ma; the Mid-Late Kimmerian phase). The area remains uplifted during the Late Jurassic till the Early Cretaceous and starts to subside gently during the Mid Cretaceous. These burial histories are generally in agreement with those of other Dutch Platforms in the offshore (e.g., De Jager, 2003, 2007; Verweij et al., 2010).

The burial histories show that the area has reached maximum burial at present day. The northern Elbow Spit Platform has undergone less burial than the rest of the area (Cleaver Bank Platform and Silverpit Platform; well E02-02; Figure 8). In the northern

and central parts of the study area, Carboniferous source rocks reached a burial depth during the Mid Jurassic that is close to their present-day burial depth (Figure 22).

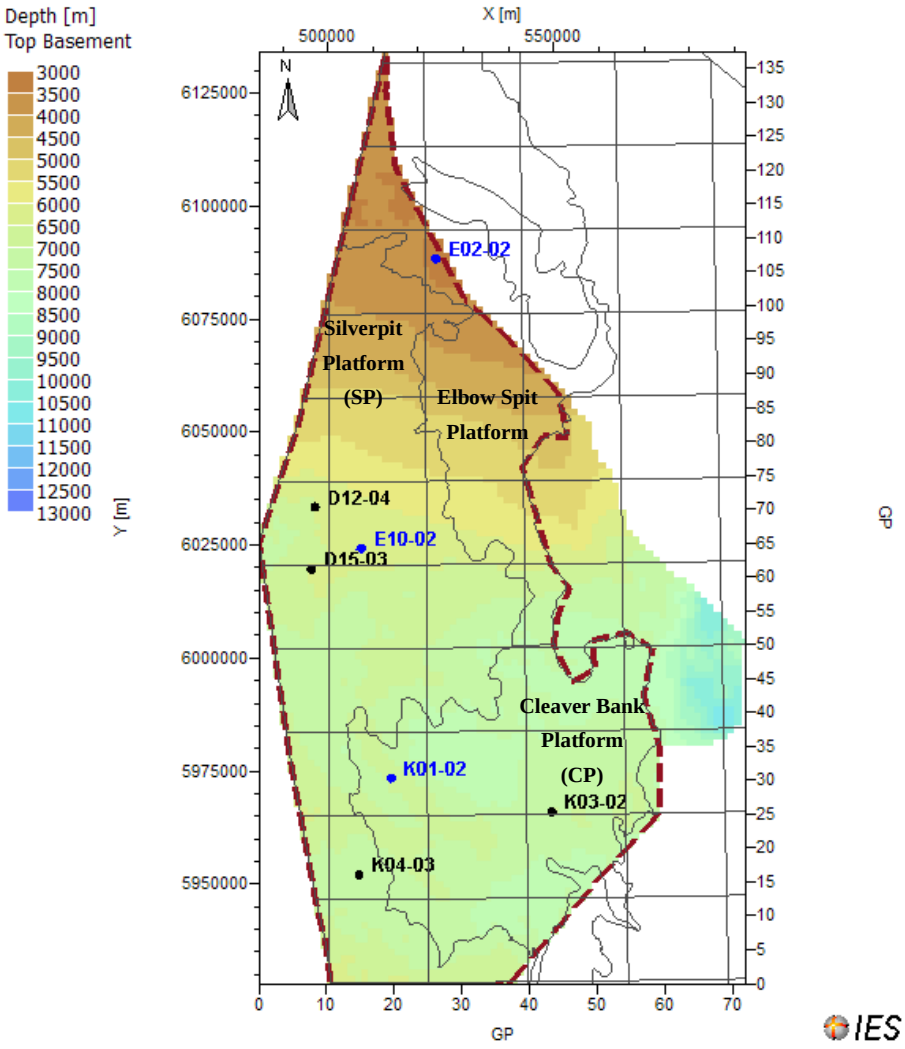

Figure 21: Map of the study area showing the location of the wells used in the study and the major structural units. Wells and 1D extractions used for burial history, temperature and maturity analysis are given the blue colour. The map overlies the depth map of the top of the Basement. Study area is delimited by dashed line.

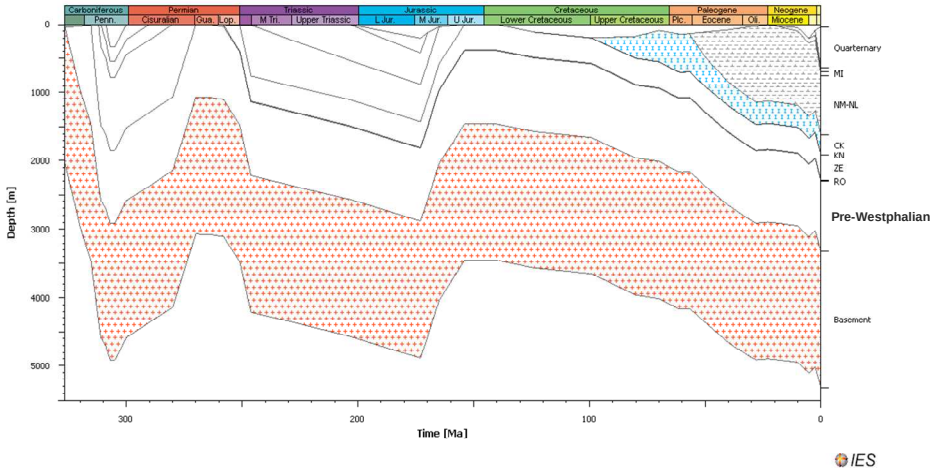

Well E02-02

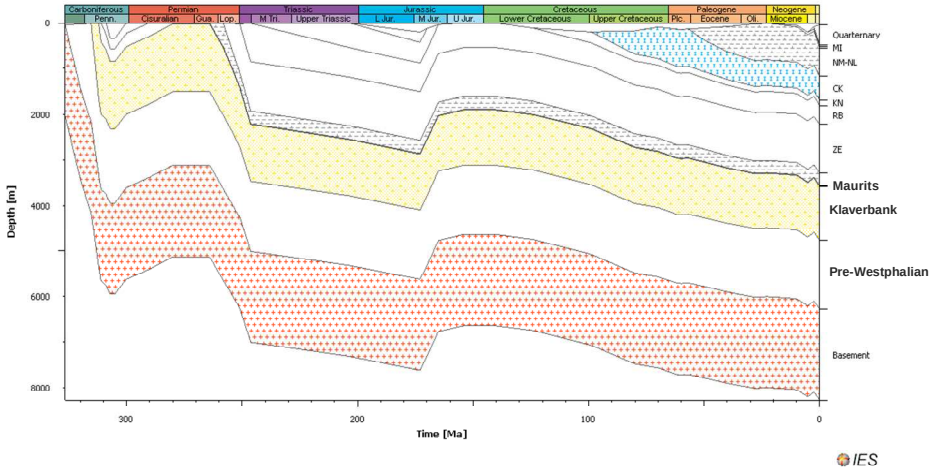

Well E10-02

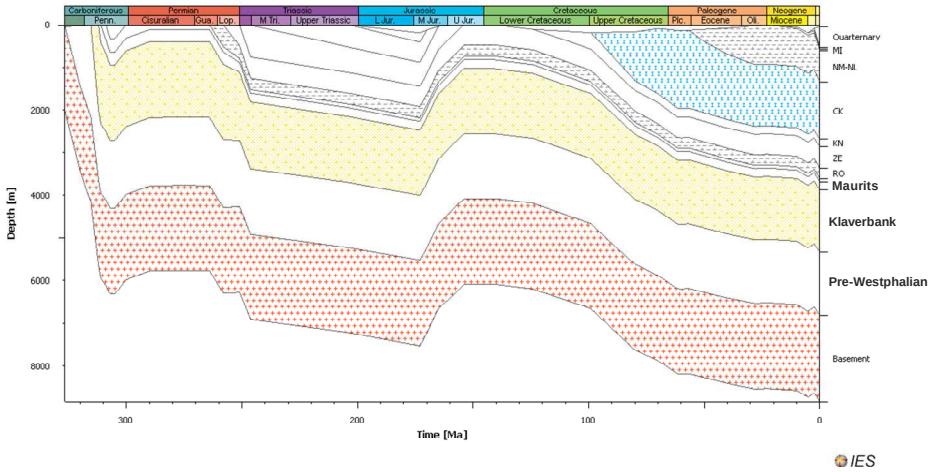

Well K01-02

Figure 22: The burial history of three 1D extractions from the 3D model. Location of the extractions is indicated in figure 21.

4.2 Thermal history

Modelled present-day temperatures in the wells E10-02 and K01-02, using the boundary conditions (Figures 10, 11, 16 & 19), show a good fit with measured temperatures (Figure 23). Figure 24 shows the modelled temperature evolution of the source rock intervals in the location of the three 1D extractions from the 3D simulation.

The simulation shows lower temperatures in the northern part of the study area (well E02-02) compared to well K01-02 and E10-02 (Figure 24). The model shows two major heating peaks at well E10-02 and well K01-02. The first maximum temperature in the Carboniferous units was reached during the Early Jurassic (prior to the Kimmerian uplift phase). The Pre-Westphalian layer reached a temperature higher than 200 °C and the temperature of the overlying Carboniferous Klaverbank and Maurits Formations ranged between 120 °C to 160 °C. During the Late Jurassic and Early Cretaceous, the temperatures of the formations decreased as a result of the Kimmerian uplift. The second high temperature phase is reached at present-day in the entire platform area. The present-day temperatures in the Namurian peak around 200 °C while they vary between 130 °C to 170 °C in the Klaverbank and Maurits Formations (Figure 24).

In well E02-02, the temperature of the Pre-Westphalian layer varied between 110 °C to 130 °C during the Late Jurassic-Early Cretaceous and at present-day. The simulation results indicate an additional temperature peak during the Late Carboniferous. The layer reached a temperature of around 130 °C prior to the Saalian uplift and erosion phase (Figure 24).

In general, burial histories show a direct relationship between the burial depth of the formations and their temperatures. The maximum temperatures are reached when the layers are at deepest burial. Hence, modelled maximum temperatures are not related to the peaks in basal heat flow that occur during the Mid-late Kimmerian uplift and erosion phase (Figures 16, 19). However, during the Miocene time, an increase in the temperature is observed that is even higher than present-day temperature. This coincides with the Miocene increase of surface temperature (Figure 11) and the slightly increasing basal heat flow (Figures 16, 19).

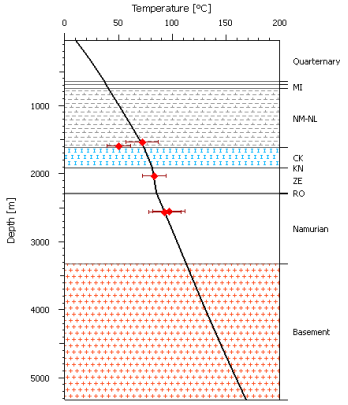

Well E02-02

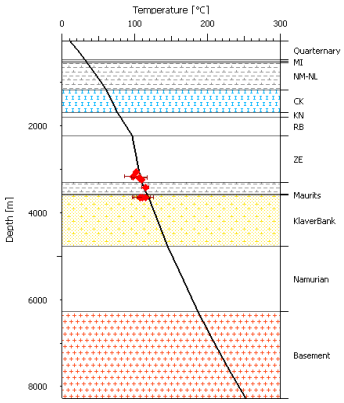

Well E10-02

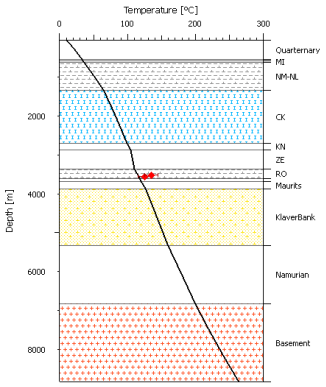

Well K01-02

Figure 23: Modelled present-day temperatures in well E10-02, well K01-02 and well E10-02 compared to measured data.

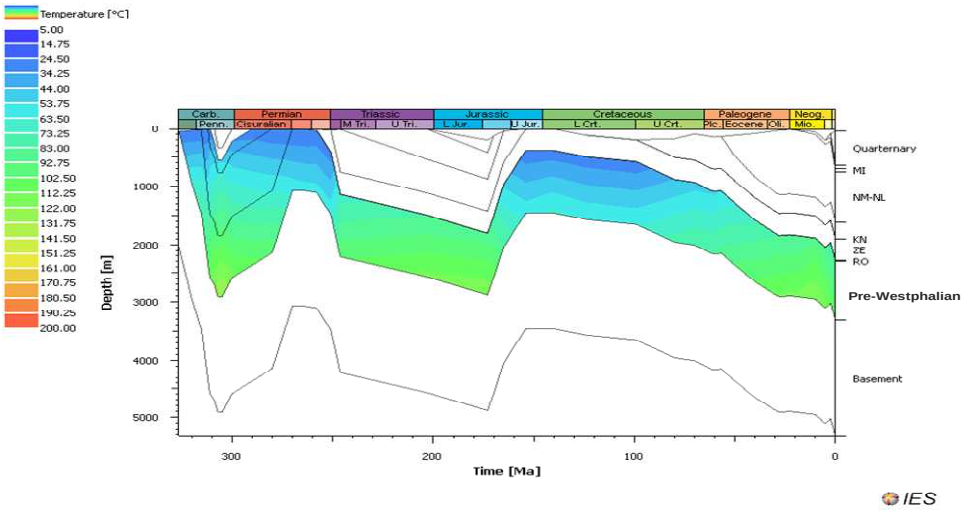

Well E02-02

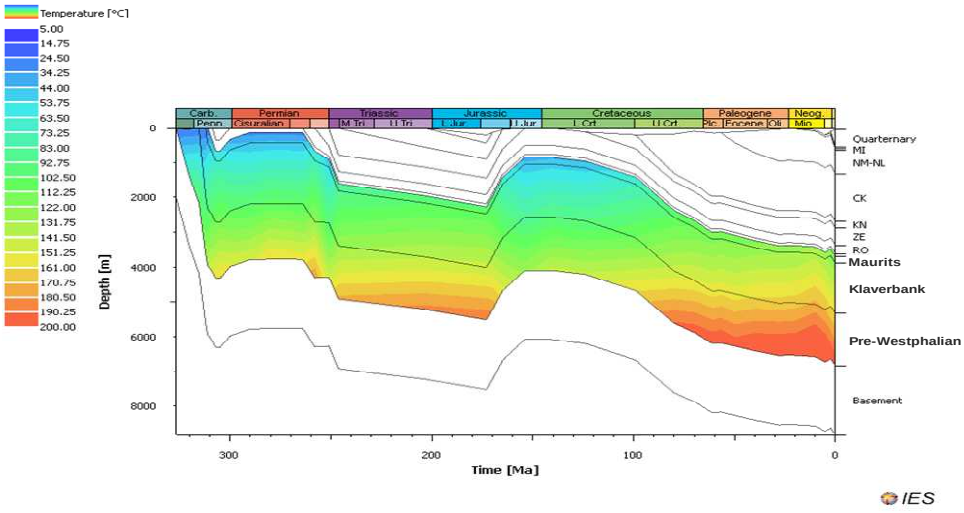

Well K01-02

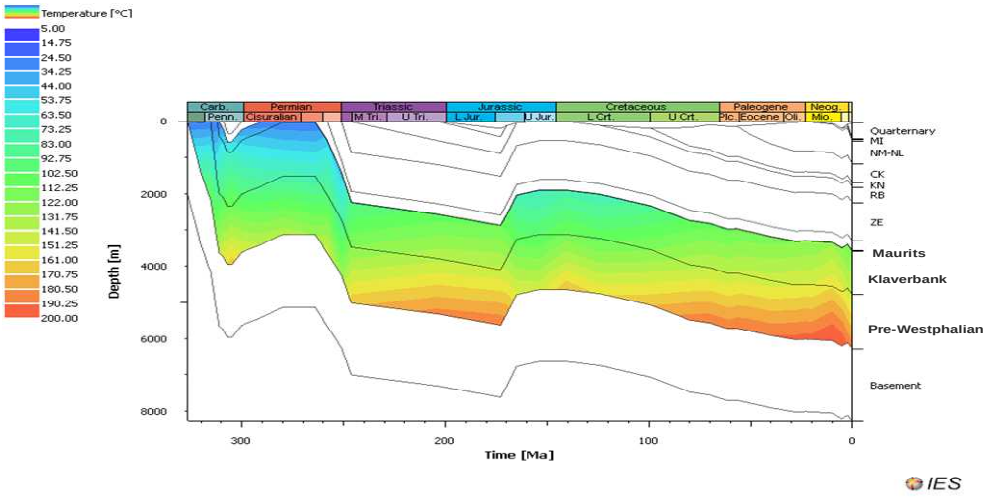

Well E10-02

Figure 24: Simulated temperature evolution for the major source rock units at thee 1D extractions from the 3D model.

4.3 History of maturity and hydrocarbon generation

PetroMod calculates maturity indicators such as vitrinite reflectance values (according to Sweeney and Burnham 1990) and transformation ratio. Vitrinite reflectance values are calculated for all stratigraphic units. The transformation ratio is the ratio of generated petroleum to the original petroleum potential in a source rock. The transformation ratio provides information on the timing of hydrocarbon generation and is calculated for the source rock units. The calculation of the transformation ratios is based on the Pepper and Corvi (1995) _TII and TIII kinetic model for the Carboniferous source rocks. Maturity history of the source rocks is directly controlled and determined by the history of the thermal regime in the area. Consequently, all parameters that influence the thermal history affect the maturity. This includes the heat flow, burial history, boundary conditions (e.g. paleo surface temperatures), proximity of salt structures and the burial history

Modelled present-day maturity, in the form of calculated vitrinite reflectance, at the location of the wells is presented in figure 25. Figure 25 indicates that the modelled maturity is in a good agreement with measured values in 7 wells covering the High and the Platform area. Modelled maturity history (vitrinite reflectance) of Carboniferous source rocks at the location of the three 1D extractions is shown in figure 26. Similar to the temperature, maturity evolution can be related to the formation depth and its burial history. The main maturity pulses occur when the formations are at their deepest burial The maturity history indicates that the deepest parts of the assigned source rock units entered the hydrocarbon generation ranges already during the Carboniferous. The maturity increased during the Triassic and reached a peak during Early Jurassic and prior to the Late Kimmerian uplift (~170 Ma). Maximum maturity is reached during Mid Jurassic in the northern part of the Elbow Spit Platform (well E02-02). The central part of the Cleaver Bank Platform (well K01-02) and the Silverpit Platform (well E10-02) reach their maximum maturity at present-day (Figure 26).

A number of variations in the degree of present-day maturity are observed over the study area (Figure 27). The Pre-Westphalian in the northern part of the study area (well E02-02) appears to be immature. The modelled maturity for this layer at this location is 0.5 - 1.3 Ro % (Figure 26, 27).

In the central and southern parts (wells E10-02 and K01-02), the Pre-Westphalian layer is currently overmature. The modelled vitrinite reflectance ranges between Ro 1.3- 4 % (Figure 27). The layer entered the gas window during the Late Carboniferous. The deeper parts of the Pre-Westphalian layer reached the overmature window in the Permian. Maturity increased during the Triassic and reached the maximum in the Late Triassic (Figure 26).

Maturity of the Klaverbank Formation varies with location and depth. The Klaverbank Formation in the Silverpit and the Elbow Spit platforms is generally in the gas window. In parts of the Cleaver Bank Platform, the formation has entered the overmature window (Figure 27). Most of the Klaverbank layer is currently in the gas generating window (Figure 26).

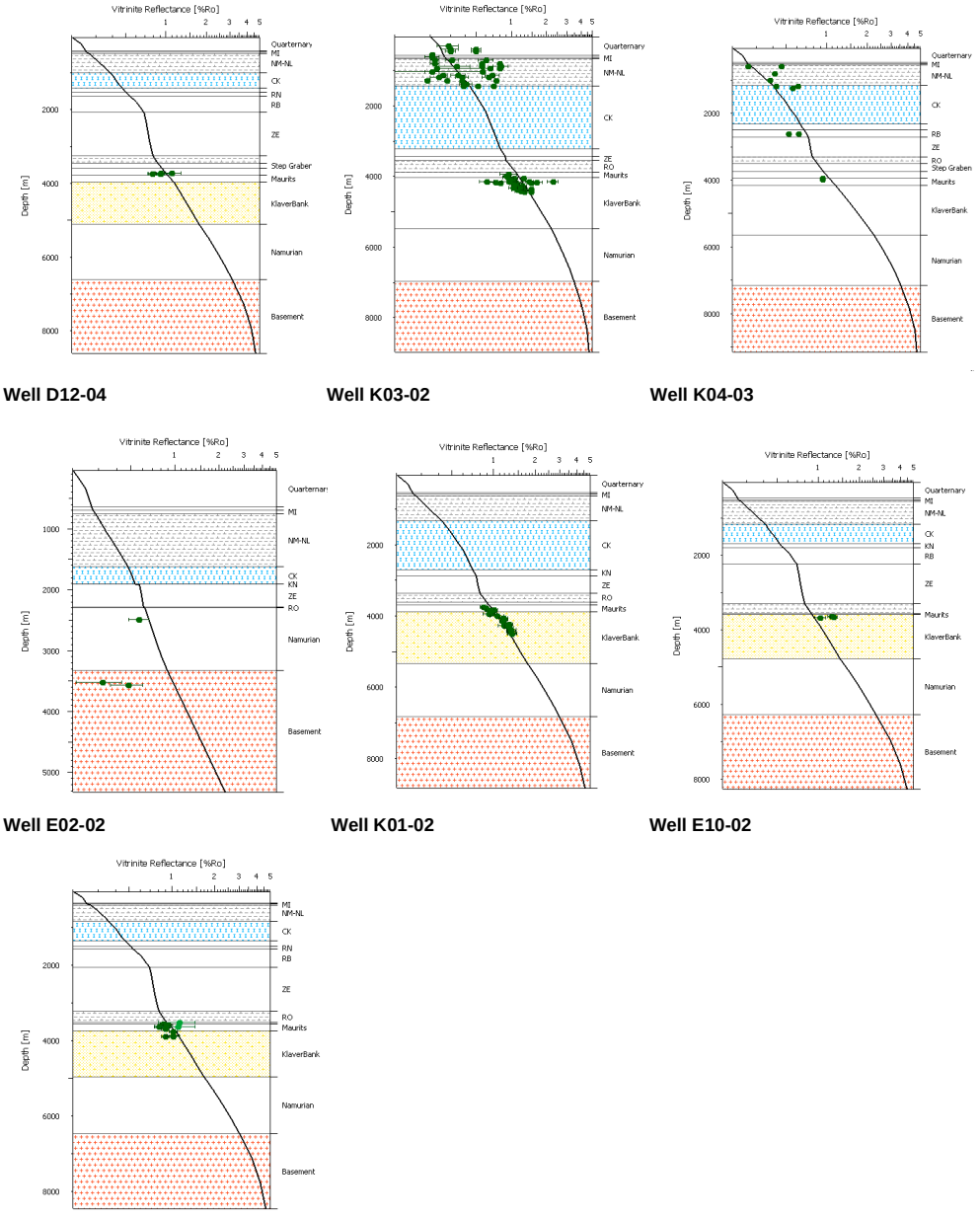

Figure 25: Modelled present-day vitrinite reflectance in 7 wells in the study area. Location of the wells is shown in figure 21.

Similar to the Pre-Westphalian layer, the maturity of the Klaverbank increased during the Late Carboniferous. It entered the generation window during the Triassic. The maturity simulations show an increase in the maturity of the Klaverbank Formation at the onset of the Paleogene. While the formation was generating gas, the deepest part became overmature (Figure 26). The model extractions show that the Maurits Formation has entered the hydrocarbon window in the Tertiary. The Maurits Formation appears to be in the gas generating window over most of the study area (Figure 27). The formation is immature in parts of the Silverpit Platform.

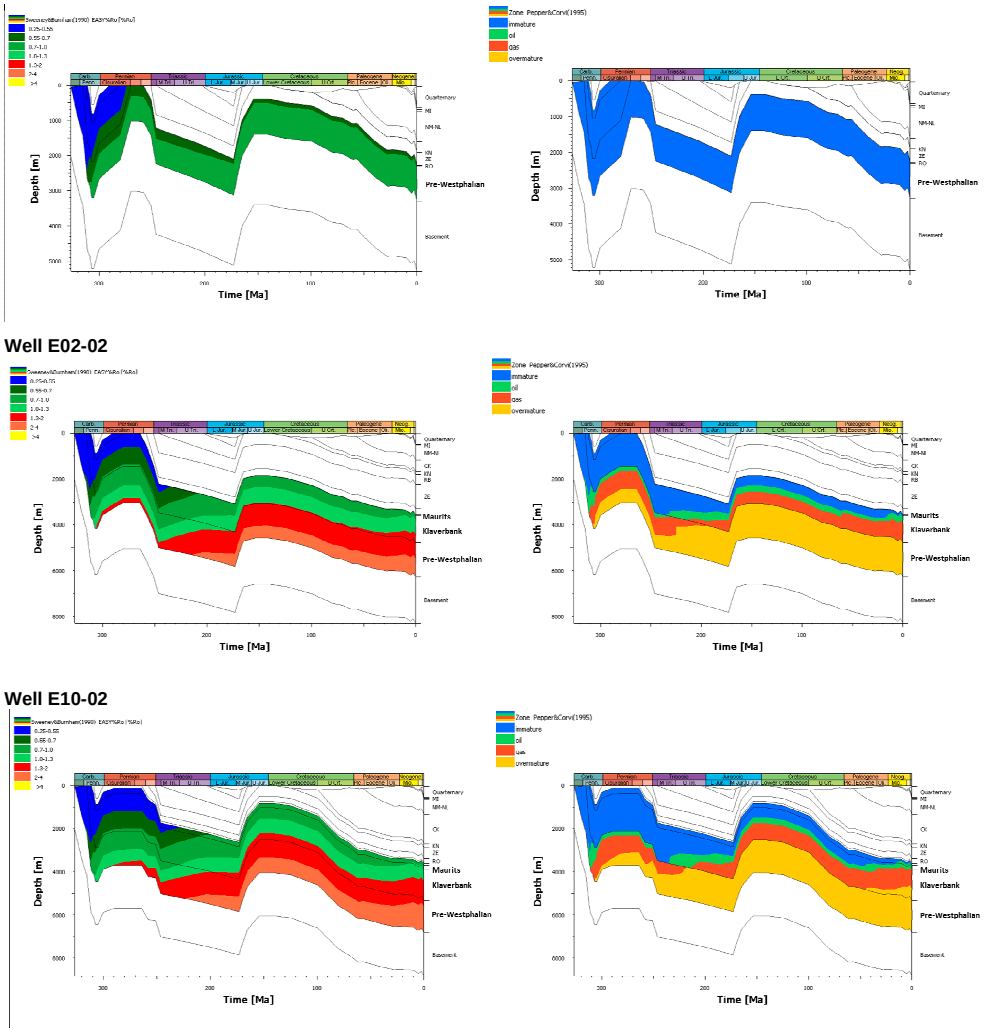

Figure 26: Modelled maturity evolution (left) and hydrocarbon generation zones (right) for the major source rock units in thee well extractions. The maturity models overly the burial histories of the thee well extractions. The proper Pepper & Corvi (1995) TIII and TII kinetics are used for the hydrocarbon generation modelling for the formations.

Figure 28 shows the transformation ratio (TR-All %) of the three Carboniferous source rocks at the location of five 1D extractions (Figure 21). A remarkable difference is observed in the transformation ratio of the Pre-Westphalian layer between the northern part and the rest of the study area. The model indicates that only a small amount of the transformable organic material is converted to hydrocarbons at well E02-02. In all other wells, however, almost all the organic material is converted to hydrocarbons at present-day (Figure 28). In all of these wells, a jump in the transformation ratio took place in the Late Carboniferous. About 80 % of the organic material in the Pre-Westphalian layer was transformed by the end of the Triassic. Maximum transformation of the Pre-Westphalian is reached at present-day (Figure 28).

The history of transformation ratio of the Klaverbank Formation shows more variations over the area and in time. Hydrocarbon generation within the Klaverbank Formation was, in some places, initiated during Early Triassic and reached a first peak in Mid Jurassic (Figure 28). The magnitude of the transformation ratio varies significantly. In

well K04-02, almost 25% of the organic material in the Klaverbank was transformed by the Mid Jurassic. This percentage did not exceed 10% in the other wells. Starting from the Late Cretaceous, the Klaverbank Formation resumed hydrocarbon generation with varying rates depending on the location. The highest ratio is observed in well K03-02 on the Cleaver Bank Platform (ca. 60%) and in well K04-03 in the southern part of the Silver Pit Platform (ca. 58%; Figure 12). Toward the north, the transformation ratio is lower and reaches a value of ca. 15% in well E10-02. An increase in the transformation ratio took place during the Miocene. This is apparent in all the 1D extractions from the study area.

According to the model, hydrocarbon generation in the Maurits Formation started in the Late Cretaceous in the whole area and reached a maximum value at present-day. Transformation ratio varies over the area with the highest values observed in well K04-03 and well K03-02 (ca. 25%). Similar to the Klaverbank Formation, the transformation ratio in the Maurits Formation decreases northwards. An increase is observed during the Miocene over the whole area (Figure 28). As with the vitrinite reflectance, the transformation ratio of the source rocks is determined by the temperature evolution of the formation. The major phases of hydrocarbon generation (Late Carboniferous, Early Mid Jurassic and the Cenozoic) are the phases that witnesses an increase in formation temperature related to deep burial (Figure 28).

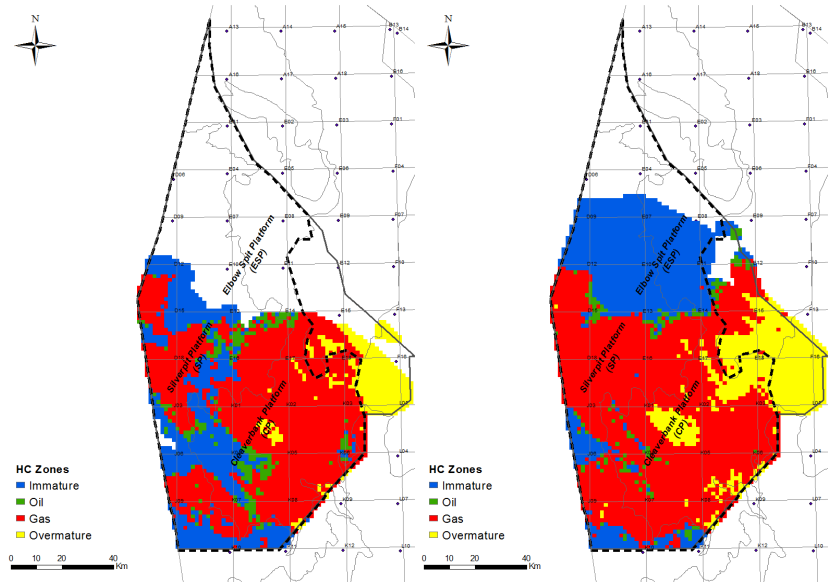

Maurits Formation **Klaverbank Formation**

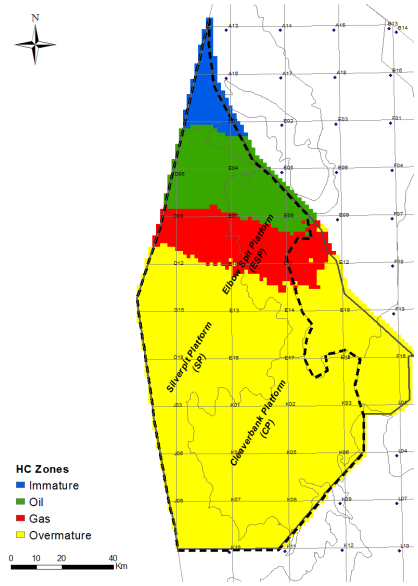

Pre-Westphalian layer

Figure 27: Hydrocarbon generation zones at the top of the Carboniferous source rocks at present-day. The Pepper & Corvi (1995) TIII kinetics is used for the Maurits, Kalverbank formations and the northern part of the Pre-Westphalian. The Pepper & Corvi (1995) TII kinetics is used for the central and southern parts of the Pre-Westphalian.

5 Discussion

Simulation of the burial history and the associated history of temperature, source rock maturity and hydrocarbon generation requires different input data and information. The latest results of the TNO mapping program is used as the basic geologic and property input for our basin modelling. In addition to uncertainties in the input geologic data, the input model is based on several assumptions, conceptual models and default set-ups.. The selection of the proper set-ups is an important part of the basin modelling workflow. Default set-ups include relations between standard lithologies and various properties such as compaction parameters, porosity-permeability relations, thermal models, kinetic models. Conceptual ideas include those related to the geological history of the area and the geo-tectonic processes that controlled its evolution.

In addition, there are uncertainties related to the quality and the background of the measurements used for calibrating the model. Basin modelling outcome, therefore, should always be evaluated and considered in the scope of the available inputs and the related uncertainties as well as the purpose of the study.

With regard to the geological model, it should be realized that the thickness maps and properties of the Carboniferous units were estimated from the base Permian subcrop map and regional information. Especially the thickness, lithostratigraphic interpretations and source rock properties of the Base Carboniferous layer are a major source of uncertainty. In the simulations we used a scenario where the entire pre-Westphalian succession, which comprises the Namurian in the south and the subcropped Dinantian in the north, is a source rock. In reality the actual presence, location and properties of the source horizons in the Pre-Westphalian in the study area is as yet largely unknown.

The simulations were run assuming that hydrostatic conditions prevail through geologic history. The development of overpressure during first burial is – through the process of disequilibrium compaction – associated with undercompaction and associated relatively high porosity of overpressured units. Current porosities in reservoir units in the study area do not show clear evidence of undercompaction. Porosity directly influences the bulk thermal conductivity and therefore the temperature and maturity history during burial. To avoid the development and preservation of unrealistic high porosities, especially in the Upper Rotliegend and Carboniferous units below the impermeable Zechstein evaporites, we decided to assume hydrostatic conditions.

The results of the modelling show are in agreement with well measurements. The modelled temperatures in two wells (E10-02, K01-02) show a good fit with the measured values in these wells (Figure 23). The fit suggests that the combination of the heat flow and the thermal conductivity of the major lithologies are acceptable. Moreover, a good fit is achieved between modelled vitrinite reflectance and the measured values in a selection of wells (Figure 25).

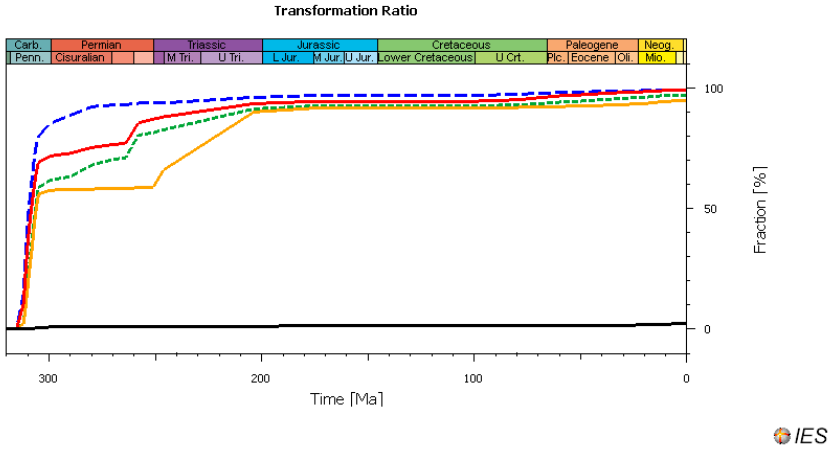

TR ALL [%] Namurian Unit

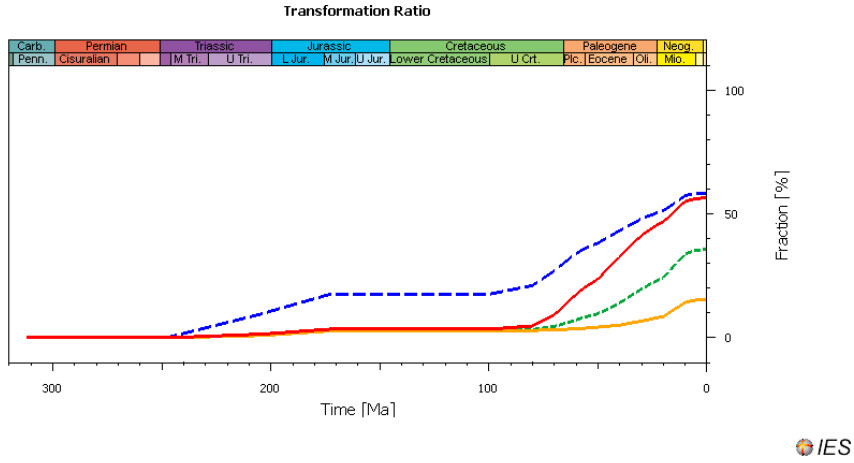

TR ALL [%] Klaverbank Formation

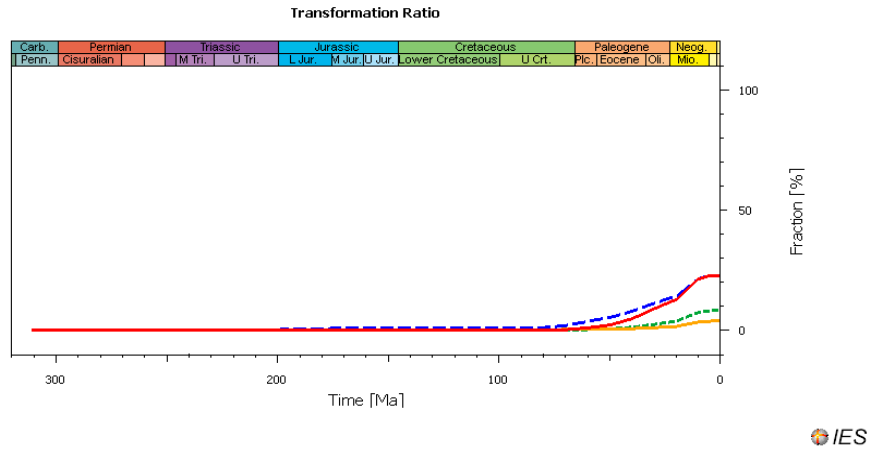

TR ALL [%] Maurits Formation

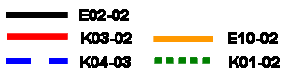

Figure 28: History of transformation ratio of the major Carboniferous source rocks in five 1D extractions. For the location of the extractions see figure 21.

Burial histories of the 1D extractions indicate that deepest burial in most of the area is at present-day. As mentioned before, an approximate burial depths of the source rocks were reached in the northern parts of the study area during the Jurassic and prior to the Mid-Late Kimmerian uplift phase (Figure 22). The assumed erosion thicknesses during the uplift phase influence the modelled maturity by affecting the burial depth of formations during the Jurassic (Figure 9). The model also shows that deep burial is reached during the Late Carboniferous in the northern part of the study area (well E02-02; Figure 22). Maturity in the north of the study area is therefore sensitive to the total erosion during the Saalian event.

As the modelled present-day maturity shows a good fit with the measurements, it is likely that the total erosion thicknesses are not significantly higher than the used values. In other words, the total thicknesses eroded during the Kimmerian uplift are not likely to be higher than the total values used in this model.

The simulation results show that the Carboniferous formations reach temperature peaks during periods of deepest burial and not necessary during heat flow peaks (Figure 16, 19 & 24). The burial history, therefore, has a more determining effect on the temperatures and maturity of the formations in this area than the variation in basal heat flow. The Pre-Westphalian succession in the centre and the south of the study area started hydrocarbon generation in the Late Carboniferous and Early Permian. It has reached maximum generation rates in the Triassic (Figure 28, 27 & 26). The whole layer in this part is overmature since the Jurassic.

In these locations, the overlying Carboniferous formations are thicker and have not completely been eroded during Saalian uplift. The Pre-Westphalian therefore went through deeper burial during the Mesozoic (Figure 26). To the north, the original thicknesses of the overlaying formations are less and the uplift and erosion is more significant. The Namurian therefore went through less burial depth and thus lower maturity (Figure 26).

The Pre-Westphalian layer in the north is in the oil generating window (Figure 28). In the northern part of the Elbow Spit Platform it appears to be immature. The calculated transformation ratio in well E02-02 is relatively low indicating very low hydrocarbon generation rates (immature source rock) (Figure 28). This can be explained by the type of organic material assigned and the applied hydrocarbon generation kinetic model. In the centre and south of the study area the Pre-Westphalian layer is considered to be uneroded Namurian. It is assigned a Namurian marine facies with organic matter of kerogen type (II). In the north, where the Namurian is eroded, the Pre-Westphalian layer is attributed the facies of the subcropped Dinantian (Figures 6, 9). A more fluvial and deltaic facies with organic matter of kerogen type (III) is assigned to this part of the layer. The Pepper and Corvi (type III) kinetic is assigned to the Dinantian facies in the northern part of the Elbow Spit Platform. This results in relatively low transformation of the organic matter even when the temperature of the layer is in the oil generation window (Figure 24, 26, 27 & 28).
The Pepper and Corvi (type II) kinetic is assigned to the Namurian facies of the Pre-Westphalian layer. This kinetics obviously has resulted in an overmature state of the source rock under the prevailing temperatures for this oil-prone source rock.
Westphalian source rocks show similar maturity history and maturity distribution patterns. Maturity and transformation ratio simulation results show that these formations are generally in the gas generating phase. The Westphalian formations

entered the overmature window in parts of the Cleaver Bank Platform (Figure 27). The maturity variations over the area are mainly caused by burial history and formation thicknesses rather than the major tectonic events. The modelled maturity and transformation rate can vary within the source rock formation. For example, the upper part of the Klaverbank Formation is generally in the gas window, the deeper parts are overmature. The same is observed for the Maurits Formation (Figure 29). This might explain the origin of gas in the known gas fields in the area.

The simulated transformation ratios of the Namurian shows that almost all of the organic matter was transformed to hydrocarbons by the end of the Triassic. Most of the generation took place during the Carboniferous and the Permian. Some gas was generated from the Namurian during the Triassic. Since the Triassic, the Namurian is overmature and very limited amount or no hydrocarbons have been generated.

Most of the generation took place before the deposition of the Zechstein, which is a main seal in the area, in the Late Permian. These gases are likely to have escaped and the Zechstein have probably sealed only gases that were generated during the Triassic. If the gas in the fields is charged from the Namurian, the generated gas (probably in the Triassic) must have been preserved after generation for the last 200 million years. The preservation has taken place either before the gas was trapped or after gas accumulation in the traps. Even though the platforms are known to be tectonically relatively quite, they have been affected by the major tectonic events (see above).

The modelled transformation ratios of the Klaverbank and Maurits formations show that hydrocarbon generation took place during the Tertiary (Figure 28). According to the model, both Westphalian formations are still producing hydrocarbons. It is therefore possible that the generated gases from the Westphalian are still preserved and thus have charged the reservoirs. The fields are, therefore, likely to be charged by gases mostly generated from Westphalian coal seams. This is not supported by the gas sample analyses which indicate more wet gases generated from marine source rock (Gerling et al., 1999; NLOG database www.nlog.nl). This contradiction regarding the source of the gas between geochemical analysis and maturity modelling requires further studies.

Nitrogen (N2) is the most abundant non-hydrocarbon gas component encountered in the accumulations of natural gases in onshore and offshore Netherlands. In the Dutch offshore, gas analyses from Rotliegend as well as Carboniferous fields in the K, J, D and E blocks show relatively high concentrations of nitrogen (Figure 30; NLOG database www.nlog.nl). The possible origin of the nitrogen in the gas accumulations in North Western Europe has been subject of extensive studies for more than 10 years (Gerling et al. 1997; Krooss et al. 1995, 2005, 2006; Littke et al. 1995; Mingram et al. 2003, 2005; Verweij, H., 2008). Although the source of nitrogen is still not very well understood, the organic material in the Westphalian coals can be an important contributor. Ammonium fixed in Namurian shales is another possible source of nitrogen.

Organic nitrogen is liberated from Westphalian coals during maturation of the kerogen. Considering the relatively low maturity, the Klaverbank and Maurits formations may still be in the early nitrogen phase which precedes the main gas generating phase (De Jager & Geluk, 2007). Early nitrogen might therefore have been generated during the Cenozoic where the Westphalian started to generate gas (Figure 28). It is not likely that

deeper parts of the Westphalian formations have entered the late nitrogen generating phase. This is because most of the formations are still in the gas generating window.

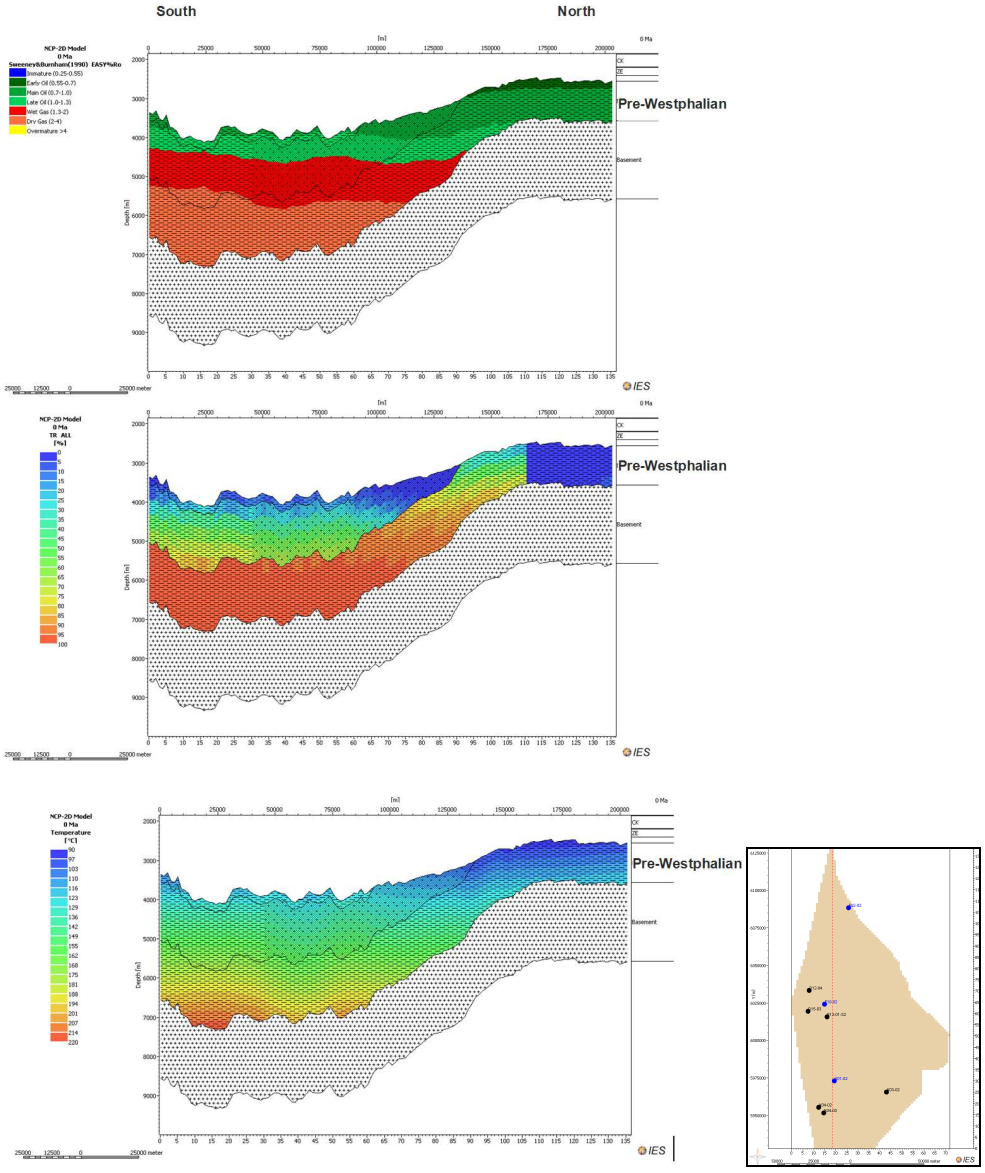

Figure 29: Cross section of the modelled maturity (top,) transformation ratio (middle) and temperature (bottom) of the Pre-Westphalian and Westphalian formations. Maturity is dependent on the depth of the formation. Maturity becomes lower to the north where the formations become shallower. The transformation ratio of the Pre-Westphalian layer in the north is because of the assigned facies and type of organic matter (kerogen III).

Pre-Westphalian formations, on the other hand, are also thought to be a possible source or nitrogen in the gas accumulations. Gerling et al. (1999) and De Jager & Geluk (2007) suggest that gas with the highest nitrogen content is generated from the pre-Westphalian marine shales. Gerling et al. (1999) propose a mixture of marine and terrestrial nitrogen in the study area.

Modelled maturity and transformation ratio suggest that Namurian source rocks started to generate hydrocarbons in the Late Carboniferous. The generation peaked in the Late Triassic (Figure 28, 26). This phase of gas generation can be associated with late nitrogen generation (De Jager & Geluk, 2007). Krooss et al. (2005) suggest that the organic matter can act as a nitrogen source up to a maturity level of 4% Vr. According to Krooss et al. (1995), late nitrogen is formed in the final stage of gas generation after methane generation has practically ceased. Experiments show that the temperature required for generating high nitrogen gases from coal samples is in the order of 300 °C (Krooss et al., 1995). This temperature exceeds what is reached in our model. However, the temperature values reported by Krooss et al. (1995) are based on laboratory tests and can differ from the necessary temperatures in subsurface conditions. Depending on the temperatures and timing of late nitrogen generation, this might have contributed to Namurian sourced nitrogen accumulation in the gas reservoirs. The release of non-organic nitrogen form shales requires relatively high temperatures (200 °C- 250 °C; Verweij, 2006; Krooss et al., 2006; Mingram et al., 2003). Our model indicates that the Pre-Westphalian layer has reached temperatures between 150 °C– 220 °C (Figure 29, 31). These temperatures might have led to the release of nitrogen from the Namurian which later accumulated in gas reservoirs.

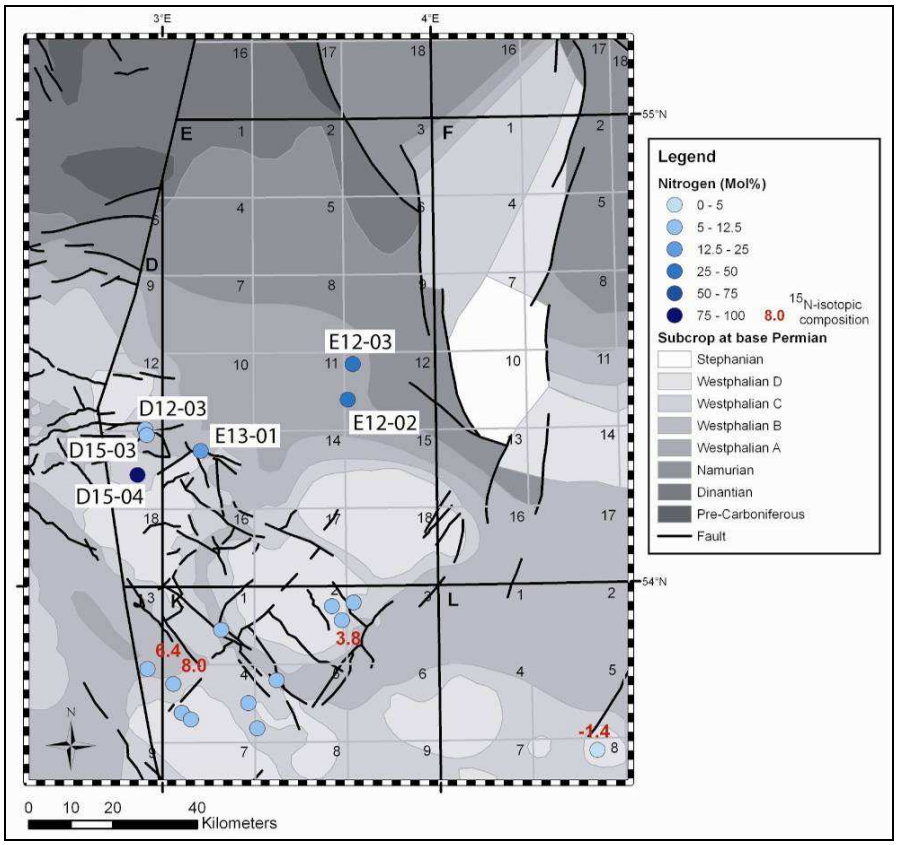

Figure 30: Variation in nitrogen content in gas accumulations in Carboniferous rocks (from Kombrink et al., 2009)

It is difficult to attribute the nitrogen concentrations in the gas fields to a specific source. The contribution of Westphalian coal seams (early nitrogen phase) is likely to be present, but not easy to distinguish from the Namurian nitrogen whether organic (late nitrogen) or non-organic. More studies are needed in order to specify different sources

of nitrogen in the gas fields. Isotope analysis of nitrogen can help segregating different nitrogen groups and identifying their sources (Gerling et al. 1997; Krooss et al. 1995, 2005, 2006; Littke et al. 1995;, 2005; Verweij, H., 2006, 2008).

The thick Namurian shale in the model can have some potential as a shale gas play. Given the thickness of the Namurian and the assigned TOC, large amounts of gas are likely to have been produced. It is difficult for the gases generated from the deepest parts of the Namurian to migrate through the thick impermeable shaly layer. The generated gas from the Namurian might therefore be trapped within the tiny pores of the thick shaly layer.
There is, however, a lot of uncertainty related to the thickness of the Namurian in our model. The introduced thickness of the Namurian is based on assumptions and conceptual models. Besides, the whole Namurian was assumed as a source rock unit with uniform distribution of organic carbon (TOC). However, assuming that the thick Namurian is a source rock and bale to produce hydrocarbon is not realistic. Hydrocarbon producing horizons are likely to be distributed within the formation and variations of the organic material within the layer are more likely. This will influence the depth of the gas generation within the unit and thus the chance of gas trapping shale pores.

In addition to that, whether or not gas has been trapped and preserved in the shales (if generated at all) also very much depends on what has happened during uplift and decrease of pressures. Based on the basin modelling we can only say something about the temperature and maturity history of the formation. More studies are required to investigate the potential of the Namurian for shale gas. Such studies will make used of the maturity and temperature models produced in this model.

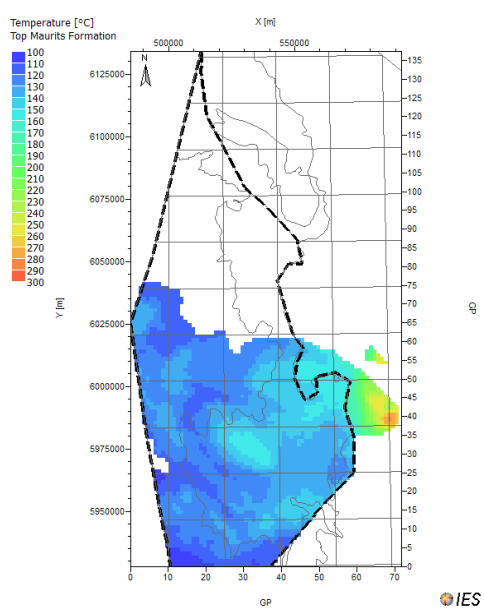

Maurits Formation

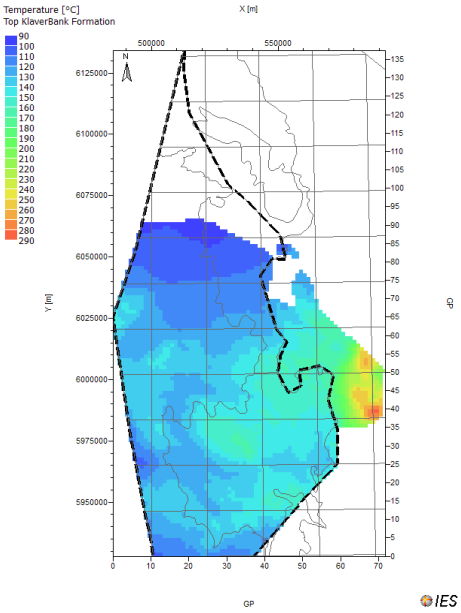

Klaverbank Formation

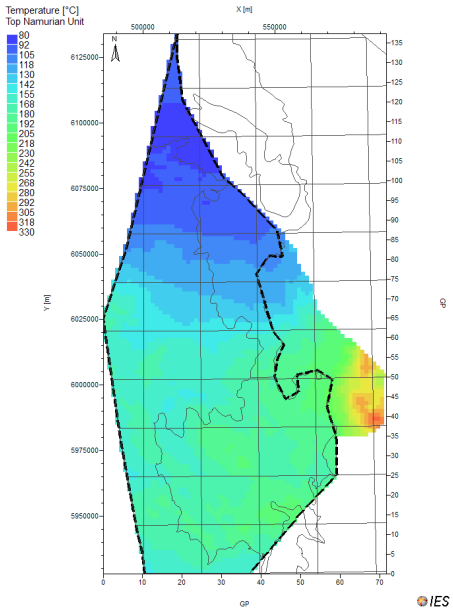

Pre-Westphalian layer

Figure 31: Temperature map at the top of the Carboniferous source rocks at present-day.

6 Conclusions

In this study, recently compiled data from the main platforms in the northwestern part of the Dutch offshore (Cleaver Bank, Silverpit and Elbow Spit Platforms) are used for a full 3D reconstruction of the burial and temperature history, source rock maturity and timing of hydrocarbon generation. The study focused on Carboniferous source rocks. The thickness distribution of the formations is based on a subcrop map of Carboniferous formations which is derived from well data. Not much is known about the thickness and the properties of the Carboniferous formations and especially the pre-Westphalian rocks in the area. The introduced thicknesses and source rock properties are speculative and are based on the limited knowledge we have thus far.

New boundary condition parameters are used in the modelling. Basal heat flow is calculated in two wells in the area based on tectonic models. Newly refined sediment water interface temperatures (SWIT) are used for maturity and temperature modelling. A recently updated and refined paleo water depth (PWD) curve is implemented in the simulation.

The 3D modelling results reveal remarkable variations in maturity and hydrocarbon generation history between the shallowest Westphalian and the assumed Pre-Wesphalian source rocks. Variations in maturity are also observed in each of the source rock units. The Pre-Westphalian source rocks started hydrocarbon generation in the Late Carboniferous and reached its maximum generation capacity in the Late Triassic. In the southern and central parts of the study area, the Namurian has been overmature since the Late Triassic and Early Jurassic. In the north, the Pre-Westphalian (Dinantian) source rocks have not generated any substantial amount of hydrocarbons. The source rock is considered to be immature. Most of the gas generation from the Namurian took place before the deposition of the Zechstein, which is main seal in the area, in Late Permian.

The Westphalian source rocks entered the gas generating window during the Early Jurassic. Maturity increase resumed during the Palaeogene because of continuous burial. Most of the Maurits and Klaverbank formations are in the gas window. The deeper parts of the formations, however, have entered the overmature window. The history of transformation ratio indicates that Westphalian formations are still generating hydrocarbons today.
It is likely that this late generation of gas from the Westphalian source rocks have contributed to the gas accumulations in the known fields. Any contribution from Namurain source rocks to the charging of gas requires the preservation of Namurian gases that were generated since the Triassic and earlier.

The simulation of temperature, maturity and hydrocarbon generation for the Carboniferous indicate that there may be different sources explaining the occurrence of nitrogen in the gas accumulations in the area. Early nitrogen may have been co-generated during the Cenozoic phase of gas generation in the Westphalian source rocks. In addition, the assumed Namurian source rock reached high temperatures and maturities corresponding to a late stage of nitrogen generation before the Kimmerian tectonic uplift phase. The temperatures reached during that time and later were also high enough to allow the release of non-organic nitrogen from Namurian shales.

Whether or not the Pre-Westphalian is a promising target for shale gas or basin centred gas exploration, primarily depend on the assessment of the actual presence and depths of source horizons in the pre-Westphalian in the platform areas. This study showed that the simulated temperature, maturity and hydrocarbon generation history at different depths in the Namurian unit indicate that major gas generation before Kimmerian uplift will have occurred provided that the source rocks are present. If so, future basin modelling studies should then focus on the preservation of the generated gas in the Namurian shales.

Finally, although the simulation results (temperatures and maturity) are consistent with measured values in wells, there is uncertainty related to the model assumptions. The distribution and thickness of the Carboniferous formations, and especially the Pre-Wesphalian succession, is a major source of uncertainty in the model. The model can be improved when more data becomes available.

Acknowledgements

We thank Schlumberger-IES for making it possible to use the basin modelling package (PetroMod Vr.11) for this study. We would also like to thank the reviewers for their valuable comments.

7 References

Allen, P.A., and Allen, J.R. 2005. Basin Analysis, Principles and Applications (second edition). Blackwell Publishing, ISBN 0-632-05207-4, p. 549.

Anonymous. 2011. NL Olie en Gasportaal. TNO Geological Survey of the Netherlands, Utrecht. Available at http:// www.nlog.nl.

Burnham, A. K. 1989. A simple kinetic model of petroleum formation and cracking. Lawrence Livermoore National Laboratory Report UCID 21665, 11 p.

De Jager, J. 2003. Inverted basins in the Netherlands, similarities and differences. Netherlands Journal of Geosciences – Geologie en Mijnbouw, 82-4, 355-366.

De Jager, J. 2007. Geological development. In: Th.E.Wong, D.A.J. Batjes and J. de Jager, eds, Geology of the Netherlands. Royal Dutch Academy of Arts and Sciences (Amsterdam), p. 5-26.

De Jager, J. and M.C. Geluk, 2007. Petroleum Geology. In: Th.E.Wong, D.A.J. Batjes and J. de Jager, eds, Geology of the Netherlands. Royal Dutch Academy of Arts and Sciences (Amsterdam), p. 241-264.

De Mulder, F.J., M.C. Geluk, I.L. Ritsema, W.E. Westerhoff and Th. E. Wong, 2003. De ondergrond van Nederland. Wolters-Noordhoff Groningen/Houten, The Netherlands, 379 p. (in Dutch).

Duin, E.J.T., J.C. Doornenbal, R.H.B. Rijkers, J.W. Verbeek and Th.E. Wong, 2006. Subsurface structure of the Netherlands - results of recent onshore and offshore mapping, Netherlands Journal of Geosciences - Geologie en Mijnbouw, v. 85-4, p. 245-276.

Donders, T.H., J.W.H. Weijers, D.K. Munsterman, M.L. Kloosterboer-van Hoeve, L.K. Buckles, R.D. Pancost, S. Schouten, J.S. Sinninghe Damsté and H. Brinkhuis, 2009. Strong climate coupling of terrestrial and marine environments in the Miocene of northwest Europe. Earth and Planetary Science Letters, v. 281, p. 215-225.

Doornenbal, J.C. and Stevenson, A.G. (editors), 2010. Petroleum Geological Atlas of the Southern Permian Basin Area. EAGE Publications b.v. (Houten).

Duin, E.J.T., J.C. Doornenbal, R.H.B. Rijkers, J.W. Verbeek and Th.E. Wong, 2006. Subsurface structure of the Netherlands - results of recent onshore and offshore mapping, Netherlands Journal of Geosciences - Geologie en Mijnbouw, v. 85-4, p. 245-276.

EBN, 2009. Focus on Dutch gas. Energie Beheer Nederland BV (EBN), Utrecht, The Netherlands, EBN report.

EBN, 2010. Annual report. Energy Beheer Nederland BV (EBN), www.ebn.nl/files/annual_report_2010.pdf

Gerling, P., Geluk, M.C., Kockel, F., Lokhorst, A., Lott, G.K. and Nicholson, R.A. 1999. 'NW European Gas Atlas' – new implications for the Carboniferous gas plays in the western part of the Southern Permian Basin. In: Fleet, A.J. & Boldy, S.A.R. (eds). Petroleum Geology of Northwest Europe: Proceedings of the 5th Conference, 799-808.

Gerling, P., Idiz, E., Everlien, G., Sohns, E. 1997. New aspects on the origin of nitrogen in natural gas in Northern Germany. Geologisches Jahrbuch D103, 65-84.

Greenwood, D.R., and S.L. Wing, 1995. Eocene continental climates and latitudinal temperature gradients. Geology, v. 23, no.11, p.1044-1048.

Hantschel, T., Kauerauf, A.I. 2009. Petroleum Generation, in Fundamentals of Basin and Petroleum Systems Modeling. Springer-Verlag Berlin Heidelberg: Berlin, ISBN978-3-540-72317-2, p. 476.

Kombrink, H., 2008. The Carboniferous of the Netherlands and the surrounding areas; a basin analysis, PhD. Thesis, University of Utrecht, Utrecht, No.294, 184 p.

Kombrink, H., Besly, B.M., Collinson, J.D., Den Hartog Jager, D.G., Drozdzewski, G., Dusar, M., Hoth, P., Pagnier, H.J.M., Stemmerik, L., Waksmundzka, M.I. & Wrede, V., 2010. Carboniferous. In: Doornenbal, J.C. and Stevenson, A.G. (editors): Petroleum Geological Atlas of the Southern Permian Basin Area. EAGE Publications b.v. (Houten): 81-99.

Kombrink, H., Della Lunga, D., Mijnlieff, H., and I. Kroon, 2009. Nitrogen contents in the northwest Netherlands offshore. TNO-report, http://www.nlog.nl/nl/pubs

Krooss, B.M., Friberg, L., Gensterblum, Y., Hollenstein, J., Prinz, D., Littke, R. 2005. Investigation of the pyrolytic liberation of molecular nitrogen from Palaeozoic sedimentary rocks. Int. J Earth Sci (Geol Rundschau), 16 p (internet version).

Krooss, B.M., Hanebeck, D., Leythaeuser, D. 1993. Experimental measurement of the molecular migration of light hydrocarbons in source rocks at elevated temperatures. In: Doré, A.G. et al. (eds). Basin modelling: Advances and applications. NPF Special Publications 3, 277-291.

Krooss, B.M., Jurisch, A., Plessen, B. 2006. Investigation of the fate of nitrogen in Palaeozoic shales of the Central European Basin. Journal of Geochemical Exploration 89, 191-194.

Krooss, B.M., Littke, R., Müller, B., Frielingsdorf, J., Schwochau, K., Idiz, E.F. 1995. Generation of nitrogen and methane from sedimentary organic matter: implications on the dynamics of natural gas accumulations. Chemical Geology 126, 291-318.

Littke, R., Krooss, B., Idiz, E. and Frielingsdorf, J. 1995. Molecular nitrogen in natural gas accumulations: Generation from sedimentary organic matter at high temperatures. AAPG Bulletin, Vol. 79 (3), 410-430.

McKenzie, D., 1978. Some remarks on the development of sedimentary basins. Earth and Planetary Science Letters, v. 40, p. 25-32.

Mingram, B., Hoth, P., Harlov, D.E. 2003. Nitrogen potential of Namurian shales in the North German Basin. Journal of Geochemical Exploration 78-79, 405-408.

Mingram, B., Hoth, P., Lüders, V., Harlov, D. 2005. The significance of fixed ammonium in Palaeozoic sediments for the generation of nitrogen-rich natural gases in the North German Basin. Int. J Earth Sci (Geol Rundschau) 94, 1010-1022.

Pepper A.S., Corvi P.J. 1995. Simple kinetic models of petroleum formation. Part III: modelling an open system. Marine and Petroleum Geology 12, 417–452.

Pharaoh, T.C., Dusar, M., Geluk, M.C., Kockel, F., Krawczyk, C.M., Krzywiec, P., Scheck-Wenderoth, M., Thybo, H., Vejbæk, O.V. & Van Wees, J.D., 2010. Tectonic evolution. In: Doornenbal, J.C. and Stevenson, A.G. (editors): Petroleum Geological Atlas of the Southern Permian Basin Area. EAGE Publications b.v. (Houten): 25-57.

Pletsch, T., Appel, J., Botor, D., Clayton, C.J., Duin, E.J.T., Faber, E., G鏅ecki, W., Kombrink, H., Kosakowski, P., Kuper, G.,Kus, J., Lutz, R., Mathiesen, A., Ostertag-Henning, C., Papiernek, B. & Van Bergen, F., 2010. Petroleum generation and migration. In: Doornenbal, J.C. and Stevenson, A.G. (editors): Petroleum Geological Atlas of the Southern Permian Basin Area. EAGE Publications b.v. (Houten): 225-253.

Quirk, D.G. 1993. Interpreting the upper Carboniferous of the Dutch Cleaver Bank High. In: J.R. Parker, Editor, Petroleum Geology of Northwest Europe: Proceedings of the 4th Conference. Geological society. London, pp.697-706.

Remmelts, G., 1996. Salt tectonics in the southern North Sea, the Netherlands. In: Rondeel, H.E., D.A.J. Batjes and W.H. Nieuwenhuijs, eds, Geology of gas and oil under the Netherlands. Kluwer, Dordrecht, p. 143-158.

Sekiguchi, K. 1984. A method for determining terrestrial heat flow in oil basinal areas. Tectonophysics v. 103, p. 67-79.

Sweeney, J.J. and A.K. Burnham, 1990. Evaluation of a simple model of vitrinite reflectance based on chemical kinetics. AAPG Bulletin, v. 74, p. 1559-1570.

TNO-NITG (Netherlands Institute of Applied Geoscience TNO – National Geological Survey), 2004. Geological Atlas of the Subsurface of The Netherlands – onshore, TNO – NITG, Utrecht, The Netherlands, 101 p.

Van Adrichem Boogaert, H.A. and W.F.P. Kouwe, eds, 1993 - 1997. Stratigraphic nomenclature of the Netherlands, revision and update by RGD and NOGEPA, Mededelingen Rijks Geologische Dienst, v. 50, The Netherlands.

Van Balen, R.T., F. van Bergen, C. de Leeuw, H. Pagnier, E. Simmelink, J-D. van Wees, and J.M. Verweij, 2000. Modelling the hydrocarbon generation and migration in the West Netherlands Basin, the Netherlands. Geologie en Mijnbouw/ Netherlands Journal of Geosciences, v. 79, p. 19-26.

Van Bergen, M.J. & Sissingh, W. 2007. Magmatism in the Netherlands: expression of the north-west European rifting history. In: Th.E.Wong, D.A.J Batjes and J. de Jager, eds, Geology of the Netherlands. Royal Dutch Academy of Arts and Sciences (Amsterdam), p. 197-221.

Van Gessel, S., H. Doornenbal, E. Duin and N. Witmans, 2008. 3D Subsurface mapping of the Dutch offshore – Results and progress. TNO Built Environment and Geosciences – National Geological Survey, Utrecht, The Netherlands. Information on GeoEnergy June 2008, p. 12-17.

Van Wees, J.D., Stephenson, R.A., Ziegler, P.A., Bayer, U., Mc-Cann, T., Dadlez, R., Gaupp, R., Narkiewicz, M., Bitzer, F. and M. Scheck. 2000. On the origin of the Southern Permian Basin, Central Europe. Marine and Petroleum Geology 17: 43–59.

Van Wees, J.D., F. van Bergen, P. David, M. Nepveu, F. Beekman, S. Cloetingh and D. Bonte, 2009. Probabilistic tectonic heat flow Modelling for basin maturation: assessment methods and applications. In: H. Verweij, M. Kacewicz, J. Wendebourg, G. Yardley, S. Cloetingh, and S. Düppenbecker, eds, Thematic Set on Basin Modelling Perspectives, Marine and Petroleum Geology, v. 26, p. 536-551.

Verweij, J.M., M. Souto Carneiro Echternach and N. Witmans, 2009b. Terschelling Basin and southern Dutch Central Graben. Burial history, temperature, source rock maturity and hydrocarbon generation - Area 2A. TNO Built Environment and Geosciences-National Geological Survey, Utrecht, The Netherlands. TNO report TNO-034-UT-2009-02065, 46 p. (report is publicly available at TNO).

Verweij, J.M., Souto Carneiro Echternach, M., Witmans, N. 2009. Central Offshore Platform - Area NCP2E, Burial history, temperature, source rock maturity and hydrocarbon generation. TNO Report, TNO-034-UT-2010-01298 / A.

Verweij, J. M., Souto Carneiro Echternach,M., Witmans, N, and Abdul Fattah, R. 2011. Reconstruction of basal heat flow, surface temperature, source rock maturity, and hydrocarbon generation in salt-dominated Dutch Basins, in: K. Peters,K., Curry,D. and M. Kacewicz, eds., Basin and Petroleum System Modeling: 2009 Napa Hedberg Conference: Hedberg Series No. 4 (in press).

Verweij, H. 2008. Isotopic signature of nitrogen: an indicator for timing N2 generation and N2 charging of Dutch natural gas accumulations. Extended abstract, 70th EAGE Conference & Exhibition, 9-12 June 2008.

Verweij, H. 2006. Nitrogen in natural gas accumulations in onshore and offshore Netherlands. TNO report available on www.nlog.nl.

Wong, Th.E., D.A.J. Batjes and J. de Jager, eds, 2007. Geology of the Netherlands. Royal Netherlands Academy of Arts and Sciences, Amsterdam, 354 p.

Zachos, J.C., G.R. Dickens, and R.E. Zeebe, 2008. An Early Cenozoic perspective on greenhouse warming and carbon-cycle dynamics. Nature, v. 451 (7176), p. 279-283.

Ziegler, P.A., 1990. Geological Atlas of Western and Central Europe (2nd edition). Shell Internationale Petroleum Maatschappij B.V.; Geological Society Publishing House (Bath): 239 pp.

8 Ondertekening

Utrecht, December 2011

Dr. M.J. van der Meulen	R. Abdul Fattah
Business Line Manager	Auteur

9 Annex

1. Basin modelling parameters, default relations
2. Heat Flow modelling parameters
3. Calibration data

1- Basin modelling parameters, default relations

Lithology-related properties and relations

Lihology	Model	Matrix thermal conductivity W/m/K	
		at 20°C	at 100°C
Chalk_100	Sekiguchi Model	2.9	2.62
Salt_100	Sekiguchi Model	6.5	5.25
Shale_100	Sekiguchi Model	1.64	1.69
Limestone_100	Sekiguchi Model	3	2.69
Sandstone_100	Sekiguchi Model	3.95	3.38
Sand/Shale_75	Sekiguchi Model	2.66	2.44
Sand/Shale_50	Sekiguchi Model	2.55	2.36
Shale/Sand_90	Sekiguchi Model	1.79	1.8
Sand/Shale_90	Sekiguchi Model	3.62	3.14
Shale/Sand_95	Sekiguchi Model	1.71	1.74
Sand/Shale_80	Sekiguchi Model	3.31	2.92
Shale/Salt_80	Sekiguchi Model	2.16	2.07
Shale/Silt_75	Sekiguchi Model	1.73	1.76
Shale/Sand_60	Sekiguchi Model	2.33	2.2
Shale/Sand_75	Sekiguchi Model	2.04	1.99
Shale/Silt/Sand/Coal_48/25/25/2	Sekiguchi Model	2.09	2.02
Shale/Sand/Coal_80/15/5	Sekiguchi Model	1.72	1.75
Basement	Sekiguchi Model	2.72	2.35

Lithology	Model	Uranium ppm	Thorium ppm	Potassium %	Porosity	Radiogenic heat production (microW/m^3)
Chalk_100	Rybach equation	1.9	1.4	0.25	0	0.6
Salt_100	Rybach equation	0.02	0.01	0.1	0	0.02
Shale_100	Rybach equation	3.7	12	2.7	0	2.03
Limestone_100	Rybach equation	1	1	0.2	0	0.35
Sandstone_100	Rybach equation	1.3	3.5	1.3	0	0.7
Sand/Shale_75	Rybach equation	0.93	3	0.68	0	0.5
Sand/Shale_50	Rybach equation	2.5	7.75	2	0	1.37
Shale/Sand_90	Rybach equation	3.46	11.15	2.56	0	1.9
Sand/Shale_90	Rybach equation	1.54	4.35	1.44	0	0.84
Shale/Sand_95	Rybach equation	3.58	11.57	2.63	0	1.97
Sand/Shale_80	Rybach equation	1.78	5.2	1.58	0	0.97
Shale/Salt_80	Rybach equation	2.96	9.6	2.18	0	1.63
Shale/Silt_75	Rybach equation	3.28	10.25	2.28	0	1.77
Shale/Sand_60	Rybach equation	2.74	8.6	2.14	0	1.5
Shale/Sand_75	Rybach equation	3.1	9.88	2.35	0	1.7
Shale/Silt/Sand/Coal_48/25/25/2	Rybach equation	2.63	7.94	1.88	0	1.4
Shale/Sand/Coal_80/15/5	Rybach equation	3.23	10.28	2.38	0	1.73
Basement	Rybach equation	0	0	0	0	0

Lithology	**Model**	**Heat Capacity Kcal/kg/K**	
		at 20°C	**at 100°C**
Chalk_100	Waples Model for Rock	0.203	0.23
Salt_100	Waples Model for Rock	0.206	0.24
Shale_100	Waples Model for Rock	0.206	0.24
Limestone_100	Waples Model for Rock	0.2	0.23
Sandstone_100	Waples Model for Rock	0.204	0.24
Sand/Shale_75	Waples Model for Rock	0.185	0.21
Sand/Shale_50	Waples Model for Rock	0.205	0.24
Shale/Sand_90	Waples Model for Rock	0.206	0.24
Sand/Shale_90	Waples Model for Rock	0.204	0.24
Shale/Sand_95	Waples Model for Rock	0.206	0.24
Sand/Shale_80	Waples Model for Rock	0.204	0.24
Shale/Salt_80	Waples Model for Rock	0.206	0.24
Shale/Silt_75	Waples Model for Rock	0.209	0.24
Shale/Sand_60	Waples Model for Rock	0.205	0.24
Shale/Sand_75	Waples Model for Rock	0.205	0.24
Shale/Silt/Sand/Coal_48/25/25/2	Waples Model for Rock	0.21	0.24
Shale/Sand/Coal_80/15/5	Waples Model for Rock	0.211	0.24
Basement	Waples Model for Rock	0.188	0.223

Lithology	Model	Initial porosity	Minimum porosity	Athy's factor km^{-1}
Chalk_100	Athy's Law (Depth)	0.7	0.01	0.9
Salt_100	Athy's Law (Depth)	0.01	0.01	0
Shale_100	Athy's Law (Depth)	0.7	0.01	0.83
Limestone_100	Athy's Law (Depth)	0.35	0.01	0.01
Sandstone_100	Athy's Law (Depth)	0.41	0.01	0.31
Sand/Shale_75	Athy's Law (Depth)	0.49	0.04	0.43
Sand/Shale_50	Athy's Law (Depth)	0.55	0.01	0.57
Shale/Sand_90	Athy's Law (Depth)	0.67	0.01	0.78
Sand/Shale_90	Athy's Law (Depth)	0.44	0.01	0.36
Shale/Sand_95	Athy's Law (Depth)	0.69	0.01	0.8
Sand/Shale_80	Athy's Law (Depth)	0.47	0.01	0.41
Shale/Salt_80	Athy's Law (Depth)	0.56	0.01	0.0769
Shale/Silt_75	Athy's Law (Depth)	0.66	0.01	0.75
Shale/Sand_60	Athy's Law (Depth)	0.58	0.01	0.62
Shale/Sand_75	Athy's Law (Depth)	0.63	0.01	0.7
Shale/Silt/Sand/Coal_48/25/25/2	Athy's Law (Depth)	0.59	0.01	0.61
Shale/Sand/Coal_80/15/5	Athy's Law (Depth)	0.66	0.01	0.73
Basement	Athy's Law (Depth)	0.05	0.05	0

Lithology	Model	Permeability (log mD) at 1% porosity	at 25% porosity
Chalk_100	Multi-Point Model	-6.75	-3.1
Salt_100	Multi-Point Model	-16	-16
Shale_100	Multi-Point Model	-8.52	-3
Limestone_100	Multi-Point Model	-2.44	2.8
Sandstone_100	Multi-Point Model	-1.8	3
Sand/Shale_75	Multi-Point Model	-5.05	1.85
Sand/Shale_50	Multi-Point Model	-5.16	0
Shale/Sand_90	Multi-Point Model	-7.85	-2.4
Sand/Shale_90	Multi-Point Model	-2.47	2.4
Shale/Sand_95	Multi-Point Model	-8.18	-2.7
Sand/Shale_80	Multi-Point Model	-3.14	1.8
Shale/Salt_80	Multi-Point Model	-10.2	-5.6
Shale/Silt_75	Multi-Point Model	-7.96	-2.5
Shale/Sand_60	Multi-Point Model	-5.83	-0.62
Shale/Sand_75	Multi-Point Model	-6.84	-1.5
Shale/Silt/Sand/Coal_48/25/25/2	Multi-Point Model	-6.16	-0.96
Shale/Sand/Coal_80/15/5	Multi-Point Model	-7.22	-2.04
Basement	Multi-Point Model	-16	-16

2- Heat flow modelling parameters

Well E10-02

LITHOLOGY(1-8)	PHI0	PHI SD	SCALE	SCALE SD	ZDEPTHCHANGE	SCALE2
SANDSTONE	41	0	2600	667	240	3300
SHALE	70	0	1280	16	750	1200
SILT	55	0	1800	621	350	2000
LIMESTONE	51	0	1900	377	1300	1900
SALT	6	0	7000	377	20000	5000
COAL	76	0	2000	377	400	1650
ANHYDRITE	6	0	7000	377	20000	5000
CARBONATE	80	0	1550	377	400	1650

Decompaction Curve Settings used in PetroProb for heat flow analysis

LITHOLOGY	CONDUCTIVITY MEAN	CONDUCTIVITY SD	COND. DISTRIBUTION	HEAT PRODUCTION MEAN	HEAT PRODUCTION SD	HEAT PROD. DISTRIBUTION
sandstone	4.15	0	Triangular	4.03e-07	0	Uniform
shale	2.35	0	Triangular	1.203e-06	0	Uniform
siltstone	2.15	0	Triangular	3.00e-07	0	Uniform
limestone	3.45	0	Triangular	2.50e-07	0	Uniform
salt	6.95	0	Triangular	1.50e-08	0	Uniform
coal	1.5	0	Triangular	0	0	Uniform
anhydrite	6.9	0	Triangular	0	0	Uniform
dolomite	4.5	0	Triangular	5.00e-07	0	Uniform
water	0.6	0	Uniform	0	0	Uniform
HC	0.5	0	Uniform	0	0	Uniform

Sediment thermal Parameters used in PetroProb for heat flow analysis

PARAMETER NAME	UNITS	VALUE mean	VALUE sd	DISTRIBUTION
lithosphere_thickness	[m]	1.150000E+05	1.0000E+04	Uniform
crust_thickness	[m]	3.0000E+04	5.000E+03	Uniform
rho0_crust	[kg/m3]	2800	0	Constant
rho0_mantle	[kg/m3]	3400	0	Constant
conductivity_crust	[-]	2.6	0	Constant
conductivity_mantle	[-]	3.4	0	Constant
heat_production_upper_crust_0means40%	[microW/m3]	0	0	Constant
heat_production_lower_crust	[microW/m3]	0.5	0	Constant
lithosphere_thermal_expansion	[-]	3.20E-05	0	Constant
base_temperature	[C]	1330	0	Constant
rho_underplate	[kg/m3]	3000	0	Constant

Lithosphere Parameters used in PetroProb for heat flow analysis

BASE FORMATION START	BASE FORMATION END	lithosphere process	iterationmode	start beta	start delta
314	DC-311	bdstretch	bdcoup	1	1
DC-erosion	DC-280	bdstretch	bfree	1	1
DC-280	265	bdstretch	bdcoup	1	1
265	249	bdstretch	bdcoup	1	1
RB-247.6	AT-203.6	bdstretch	bdcoup	1	1
AT-erosion	KN-154	bdstretch	bfree	1	1
132	92.9	bdstretch	bdcoup	1	1
50	44.7	bdstretch	bdcoup	1	1
44.7	20.43	bdstretch	bdcoup	1	1
20.43	5.33	bdstretch	bdcoup	1	1
5.33	PD	bdstretch	bdcoup	1	1

Tectonic model used in PetroProb for heat flow analysis

Well K01-02

LITHOLOGY(1-8)	PHI0	PHI SD	SCALE	SCALE SD	ZDEPTHCHANGE	SCALE2
SANDSTONE	41	0	2600	667	240	3300
SHALE	70	0	1280	16	750	1200
SILT	55	0	1800	621	350	2000
LIMESTONE	51	0	1900	377	1300	1900
SALT	6	0	7000	377	20000	5000
COAL	76	0	2000	377	400	1650
ANHYDRITE	6	0	7000	377	20000	5000
CARBONATE	80	0	1550	377	400	1650

Decompaction Curve Settings used in PetroProb for heat flow analysis

LITHOLOGY	CONDUCTIVITY MEAN	CONDUCTIVITY SD	COND. DISTRIBUTION	HEAT PRODUCTION MEAN	HEAT PRODUCTION SD	HEAT PROD. DISTRIBUTION
sandstone	4	0	Triangular	4.03e-07	0	Uniform
shale	1.9	0	Triangular	1.203e-06	0	Uniform
siltstone	2.1	0	Triangular	3.00e-07	0	Uniform
limestone	3.1	0	Triangular	2.50e-07	0	Uniform
salt	6.8	0	Triangular	1.50e-08	0	Uniform
coal	1	0	Triangular	0	0	Uniform
anhydrite	6.75	0	Triangular	0	0	Uniform
dolomite	4.4	0	Triangular	5.00e-07	0	Uniform
water	0.6	0.0	Uniform	0	0	Uniform
HC	0.5	0.0	Uniform	0	0	Uniform

Sediment thermal Parameters used in PetroProb for heat flow analysis

PARAMETER NAME	UNITS	VALUE mean	VALUE sd	DISTRIBUTION
lithosphere_thickness	[m]	1.15000E+05	1.0000E+04	Uniform
crust_thickness	[m]	3.4000E+04	5.000E+03	Uniform
rho0_crust	[kg/m3]	2800	0	Constant
rho0_mantle	[kg/m3]	3400	0	Constant
conductivity_crust	[-]	2.6	0	Constant
conductivity_mantle	[-]	3.4	0	Constant
heat_production_upper_crust_0means40%	[microW/m3]	0	0	Constant
heat_production_lower_crust	[microW/m3]	0.5	0	Constant
lithosphere_thermal_expansion	[-]	3.20E-05	0	Constant
base_temperature	[C]	1330	0	Constant
rho_underplate	[kg/m3]	3000	0	Constant

Lithosphere Parameters used in PetroProb for heat flow analysis

BASE FORMATION START	BASE FORMATION END	lithosphere process	iterationmode	start beta	start delta
314.0	DC-311	bdstretch	bdcoup	1	1
DC-erosion	DC-280	bdstretch	bfree	1	1
267.5	RB-251	bdstretch	bdcoup	1	1
RB-251	AT-203	bdstretch	bdcoup	1	1
AT-203	AT-erosion	bdstretch	bdcoup	1	1
AT-erosion	138.8	bdstretch	bfree	1	1
138.8	90.4	bdstretch	bdcoup	1	1
90.4	54.0	bdstretch	bdcoup	1	1
54.0	50.0	bdstretch	bdcoup	1	1
50.0	24.0	bdstretch	bdcoup	1	1
24.0	5.33	bdstretch	bdcoup	1	1
5.33	PD	bdstretch	bdcoup	1	1

Tectonic model used in PetroProb for heat flow analysis

3 - Calibration data

Temperature and vitrinite reflectance data used for Heat Flow Calibration

Well E10-02

Temperature

Measured Depth [m]	Corrected Temperature [C]	Minimum Temperature [C]	Maximum Temperature [C]	Quality
2224	83.63	72.63	94.63	BHT
2234	83.63	72.63	94.63	BHT
3299	102	100	104	DST
3465	114.21	103.21	125.21	BHT
3465	96.95	85.95	107.95	BHT
3466	106.2	95.2	117.2	BHT
3472	106.2	95.2	117.2	BHT
3477	106.2	95.2	117.2	BHT
3506	109.1	107.1	111.1	DST
3697	114	109	119	DST
3958	109.84	98.84	120.84	BHT
3959	106.95	95.95	117.95	BHT
3961	114.21	103.21	125.21	BHT

Vitrinite reflectance

Measured Depth [m]	Value [%Ro]	Minimum Value [%Ro]	Maximum Value [%Ro]	Quality
3961	1.25	1.17	1.33	Good
3972	1.3	1.23	1.37	Medium
3999	1.04	0.95	1.13	Medium

Well K01-02

Vitrinite reflectance

Measured Depth [m]	Value [%Ro]	Minimum Value [%Ro]	Maximum Value [%Ro]	Quality
3746	0.85	0.8	0.9	Medium-Poor
3792	0.89	0.83	0.95	Medium-Poor
3824	1	0.94	1.06	Medium-Poor
3854	0.94	0.88	1	Medium-Poor
3906	0.98	0.91	1.05	Medium-Poor
3950	0.93	0.84	1.02	Medium-Poor
4002	1.06	0.94	1.18	Medium-Poor
4068	1.18	1.09	1.27	Medium-Poor
4102	1.19	1.12	1.26	Medium-Poor
4168	1.17	1.1	1.24	Medium-Poor
4228	1.29	1.21	1.37	Medium-Poor
4278	1.19	1.08	1.3	Medium-Poor
4278	1.28	1.2	1.36	Medium-Poor
4326	1.29	1.19	1.39	Medium-Poor
4388	1.34	1.23	1.45	Medium-Poor
4434	1.34	1.24	1.44	Medium-Poor
4482	1.36	1.25	1.47	Medium-Poor
4504	1.36	1.26	1.46	Medium-Poor

Temperature

Measured Depth [m]	Corrected Temperature [C]	Minimum Temperature [C]	Maximum Temperatur e [C]	Quality
3546	135	130	140	DST
3625	125	118	133	DST
1464.84	55	44	66	BHT
2904.47	84	73	95	BHT
2906.46	84	73	95	BHT
3624.27	116	105	127	BHT
3624.28	112	101	123	BHT
3625.27	109	98	120	BHT
3625.77	106	95	117	BHT
3949.84	138	127	149	BHT
4101.02	137	126	148	BHT
4102.42	134	123	145	BHT
4194.15	129	118	140	BHT
4392.98	138	127	149	BHT
4392.99	142	131	153	BHT
4498.87	149	138	160	BHT
4502.87	149	138	160	BHT
4504.87	149	138	160	BHT

4504.88	149	138	160	BHT
4506.87	146	135	157	BHT
4525.85	147	136	158	BHT
4525.86	146	135	157	BHT

Temperature and vitrinite reflectance data used for calibrating maturity models

Well K04-02				
Measured Depth [m]	**Value [%Ro]**	**Min [%Ro]**	**Ma [%Ro]**	**Quality**
3720	0.94	0.93	0.95	Medium
3729	0.91	0.91	0.91	Poor
3729	0.91	0.91	0.91	Poor
3759	0.83	0.74	0.92	Medium
3759	1.42	1.42	1.42	Poor
3825	0.93	0.93	0.93	Poor
3879	0.89	0.85	0.93	Medium
3888	0.99	0.99	0.99	Poor

Well E13-01-S2				
Measured Depth [m]	**Temperature [°C]**	**Min Temperature [°C]**	**Max Temperature [°C]**	**Quality**
3204	101.68	96.68	106.68	Good
3527	106.45	101.45	111.45	Good
3604	110.23	105.23	115.23	Good
3622	109.4	104.4	114.4	Good
3659	111.95	106.95	116.95	Good
3712	112.45	107.45	117.45	Good
3766	112.95	107.95	117.95	Good
3925	116.68	111.68	121.68	Good
3988	118.07	113.07	123.07	Good
3715	105	98	113	Medium
4016	105	98	113	Medium
2115	66	55	77	Poor
3714	94	83	105	Poor
4015	96	85	107	Poor
4018	108	97	119	Poor

Well E13-01-S2				
Measured Depth [m]	Value [%Ro]	Min [%Ro]	Ma [%Ro]	Quality
1867	0.81	0.6	1.02	Poor
1887	0.99	0.41	1.57	Poor
1967	0.84	0.71	0.97	Medium
2007	0.84	0.77	0.91	Poor
1987	0.66	0.51	0.81	Poor
2357	1.01	0.95	1.07	Good

Well D15-03				
Measured Depth [m]	Value [%Ro]	Min [%Ro]	Ma [%Ro]	Quality
3541	1.13	0.8	1.46	Medium
3585	0.87	0.82	0.92	Medium
3615	0.89	0.83	0.95	Medium
3919	0.9	0.84	0.96	Medium
3620	0.94	0.87	1.01	Medium
3620	0.91	0.83	0.99	Medium
3656	0.81	0.75	0.87	Medium
3663	1.11	0.76	1.46	Medium
3715	0.9	0.84	0.96	Medium
3795	1.02	0.95	1.09	Medium
3905	1.02	0.92	1.12	Medium
3914	1.02	0.9	1.14	Medium

Well K03-02				
Measured Depth [m]	Value [%Ro]	Min [%Ro]	Ma [%Ro]	Quality
344	0.29	0.23	0.35	Poor
435	0.3	0.25	0.35	Poor
435	0.5	0.45	0.55	Poor
496	0.3	0.27	0.33	Poor
496	0.5	0.45	0.55	Poor
588	0.21	0.2	0.22	Poor
649	0.21	0.18	0.24	Poor
740	0.31	0.27	0.35	Poor
740	0.22	0.2	0.24	Poor
740	0.61	0.52	0.7	Poor
831	0.22	0.2	0.24	Poor
831	0.56	0.56	0.56	Poor
831	0.8	0.8	0.8	Poor
923	0.34	0.24	0.44	Poor
923	0.56	0.55	0.57	Poor
923	0.82	0.7	0.94	Poor
984	0.23	0.23	0.23	Poor
984	0.66	0.66	0.23	Poor

984	0.8	0.8	0.8	Poor
1075	0.21	0.18	0.24	Poor
1075	0.57	0.56	0	Poor
1167	0.35	0.3	0.4	Poor
1167	0.26	0.24	0.28	Poor
1167	0.69	0.59	0.79	Poor
1228	0.38	0.33	0.43	Poor
1228	0.24	0.2	0.28	Poor
1228	0.64	0.56	0.72	Poor
1319	0.38	0.38	0.38	Poor
1319	0.19	0.18	0.2	Poor
1319	0.28	0.28	0.28	Poor
1319	0.75	0.75	0.75	Poor
1411	0.41	0.36	0.46	Poor
1472	0.39	0.37	0.41	Poor
1472	0.52	0.52	0.52	Poor
1472	0.71	0.68	0.74	Poor
3965	0.95	0.8	1.1	Poor
4038	0.92	0.85	0.99	Poor
4062	0.94	0.84	1.04	Poor
4087	1.06	0.98	1.14	Poor
4087	1.28	1.22	1.34	Poor
4111	0.97	0.92	1.02	Poor
4148	1.02	0.92	1.12	Poor
4184	0.97	0.83	1.11	Poor
4184	0.62	0.53	0.71	Poor
4184	1.43	1.32	1.54	Poor
4184	2.29	2.04	2.54	Poor
4209	1.06	0.91	1.21	Poor
4209	0.74	0.65	0.83	Poor
4209	1.66	1.47	1.85	Poor
4233	1.11	0.95	1.27	Poor
4233	0.81	0.77	0.85	Poor
4233	1.49	1.46	1.52	Poor
4257	1.08	0.98	1.18	Poor
4306	1.25	1.15	1.35	Poor
4331	1.15	1.01	1.29	Poor
4355	1.04	0.95	1.13	Poor
4379	1.19	1.09	1.29	Poor
4404	1.26	1.15	1.37	Poor
4404	1.49	1.45	1.53	Poor
4428	1.13	1	1.26	Poor
4452	1.21	1.08	1.34	Poor
4477	1.3	1.22	1.38	Poor
4477	1.49	1.44	1.54	Poor